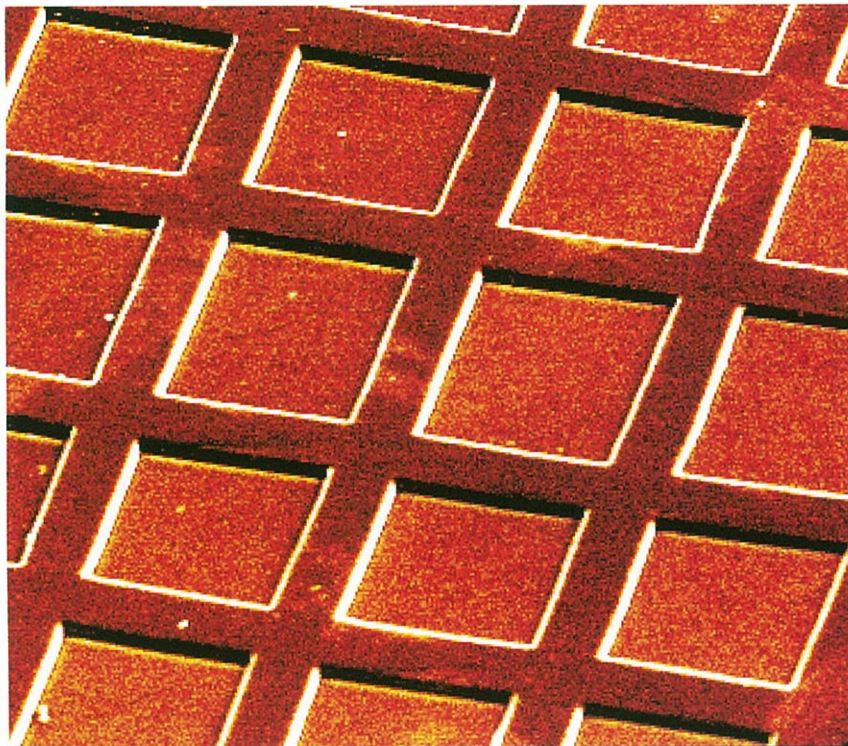

Surface and Photochemistry

BL2B1, 3A1, 4A1, 4A2, 5B, 6B, 8A

Ideal H-terminated Si(100) Surface Formation By Dry Process And Its Reactive Properties

Zhihong Wang[1], Hideyuki Noda [1], Youichi Nonogaki[2] and Tsuneo Urisu [2]
([1]The Graduate University for Advanced Studies, [2]Institute for Molecular Science)

The preparation of ideal Si(100) surfaces which are free of contamination and defects is important in both the fields of semiconductor device fabrication technology and surface science. The wet treatment using HF solution can only provides ideal H-terminated Si(111) surfaces, but it results in rough Si(100) surfaces. Concerning H-terminated Si(100) surfaces, we have found that they are very stable under synchrotron irradiation. However, the chemical stability against contamination is not well known. In this work, an ideal H-terminated Si(100) surface prepared in ultrahigh vacuum by the dry process is monitored with BML-IRRAS to investigate the chemical stability of the surface. Figure 1 shows the dependence of the coupled Si-H symmetric stretching peak integrated absorbance (IA) and its peak position on the adsorption temperatures. Figure 2 shows the adsorption temperature dependence of the peaks width. If we assume that the coverage θ of the Si-H at the stationary state is given by $\theta = \Gamma /(k+\Gamma)$, (k and Γ are the desorption and the adsorption rate, respectively). The coverage θ of Si-H is calculated by fitting the equation to the observed IA and using the reported activation energy 2.82eV for k as show in Fig. 1. From these data, it is concluded that the ideal H-terminated surface is given at the temperature range T≈400 ~ 440 °C (θ >0.99). The chemical stability of this surface for the H_2O and D_2O exposures is going to be investigated.

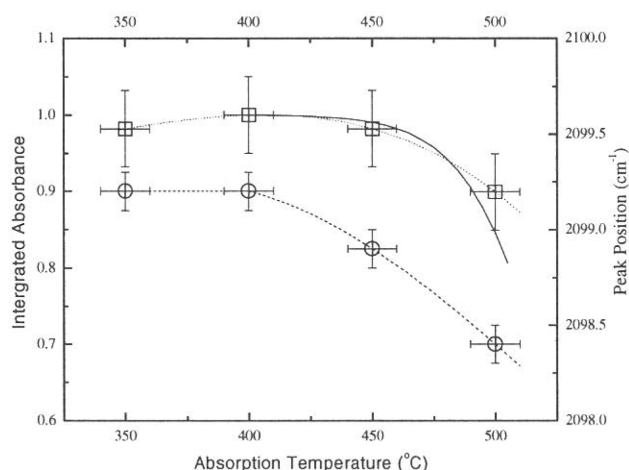

Fig.1 Dependence of IA(□) and the peak position(○) of the Si-H symmetric stretching peak on the hydrogen atom adsorption. ------: smoothly fitted line, —— : calculated coverage of Si-H. IA is normalized to 1 at the maximum.

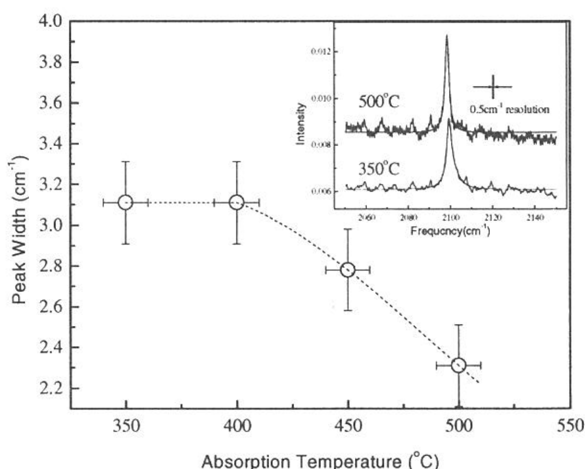

Fig. 2 Dependence of the peak width of the Si-H symmetric stretching peak on the hydrogen atom adsorption temperature.
Inserted figure is the observed IR spectra.

(BL2B1)

Layer-Resolved Auger Spectra of $CF_3CD(OH)CH_3$ on a Si(100) Surface

Shin-ichi NAGAOKA, Arinobu NAKAMURA,[A] Kazuhiko MASE[B] and Shin-ichiro TANAKA[C]

Institute for Molecular Science, Okazaki 444-8585

[A]*Department of Chemistry, Faculty of Science, Ehime University, Matsuyama 790-8577*

[B]*Photon Factory, Institute of Materials Structure Science, High Energy Accelerator Research Organization, 1-1 Oho, Tsukuba 305-0801*

[C]*Department of Physics, Graduate School of Science, Nagoya University, Chikusa-ku, Nagoya 464-8602*

The study of adsorbate properties and behaviors on substrates has attracted considerable attention. Chiang et al. previously reported the observation of layer-resolved shifts of photoemission spectra from physisorbed rare-gas multilayers [1]. The shifts were explained in terms of difference in final-state hole-screening energy. We previously studied the photoelectron spectra (PES) of $CF_3CD(OH)CH_3$ (TFIP-d_1) on Si(100) and found that similar shifts can be revealed in the binding energies of the C:1s core-level, the O:1s core-level and the valence level [2]. In the present study, we have studied the Auger spectra of TFIP-d_1 on Si(100) and found that similar shifts are also evident in the Auger spectra.

TFIP-d_1 was prepared with the reaction of CF_3COCH_3 and $LiAlD_4$. The amount-regions of gas exposure corresponding to the monolayer coverage and the multiplayer coverage were determined by observing the development of the ion intensity as a function of the amount of gas exposure; the plot of the ion intensity versus the amount of gas exposure was discontinuous between the two regions. The experiments were performed using a double-pass cylindrical-mirror electron-energy analyzer (ULVAC-PHI) and a home-built time-of-flight ion-detection assembly coupled to a grasshopper monochromator (Mark XV) installed on the BL2B1 beamline [3].

Figures 1a-3a show the C, O and F:KVV normal Auger spectra (NAES) of TFIP-d_1 monolayer and multiplayer on a Si(100) surface. Figures 1b-3b show the C, O and F:KVVσ^* resonant Auger spectra (RAES) . The peaks in the spectrum of the multilayer are shifted to lower kinetic energies from those of the monolayer. The absolute values of the shift are summarized in Table 1. As in the case of rare-gas [1], the shift in NAES is three times as large as that in the corresponding PES, and thus can be explained in terms of difference in final-state hole-screening energy.

Further investigations on the site-specific fragmentation in TFIP-d_1 [4,5] are in progress.

Table 1 Spectral shift in eV between monolayer and multiplayer

	PES	NAES	RAES
C:1s	0.5	1.5	0.7
O:1s	0.5	1.5	0.7
F:1s	<0.3	0.6	0.4

[1] T.-C. Chiang, G. Kaindl and T. Mandel, Phys. Rev. B **33**, 695 (1986).

[2] S. Nagaoka, A. Nakamura, K. Mase and S. Tanaka, UVSOR Activity Report, **27**, 120 (1999).

[3] S. Tanaka, N. Takahashi, K.-P. Lee and M. Kamada, J. Electron Spectrosc. Relat. Phenom. **80**, 205 (1996).

[4] A. Nakamura, S. Nagaoka, K. Mase, S. Tanaka and T. Urisu, UVSOR Activity Report, **26**, 100 (1998).

[5] K. Mase, S. Tanaka, S. Nagaoka and T. Urisu, Surf. Sci. **451**, 143 (2000).

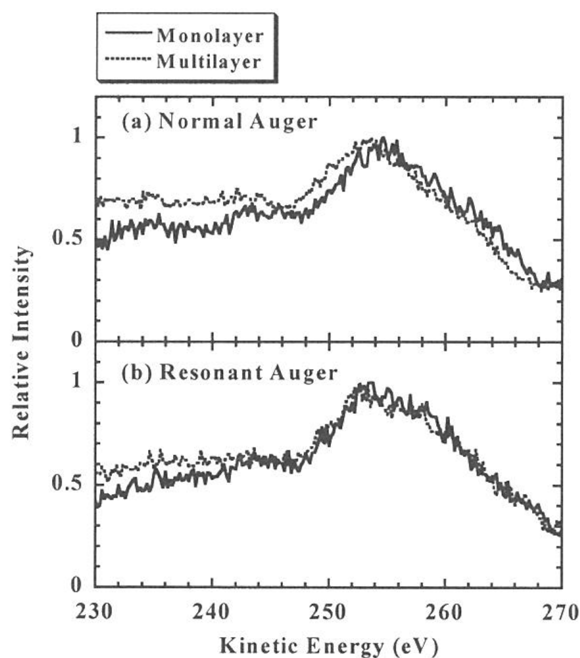

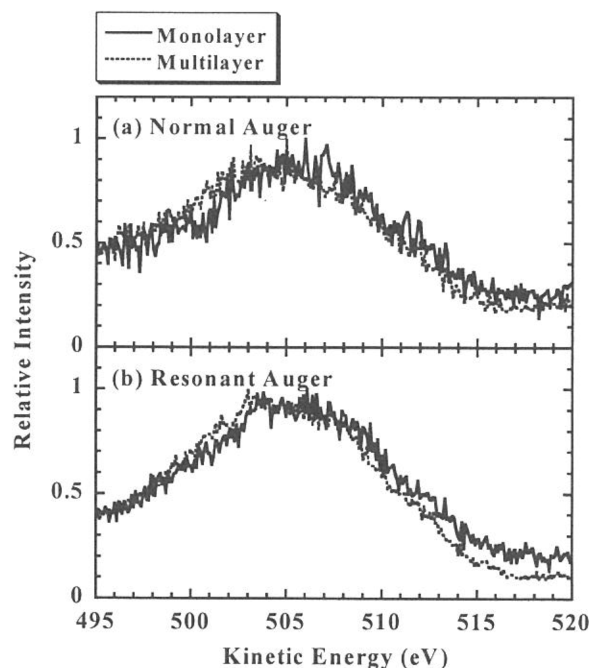

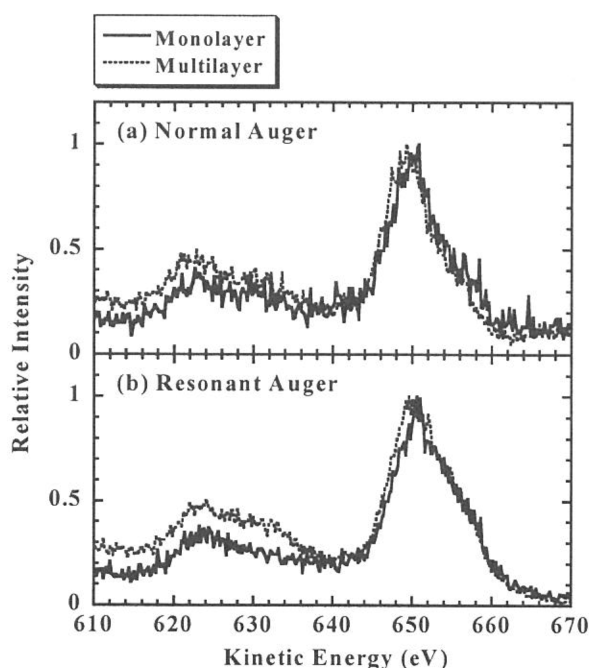

Figure 1 (upper left-hand side). C:1s Auger spectrum of TFIP-d_1 on a Si(100) surface. (a) KVV NAES. (b) KVVσ^* RAES.

Figure 2 (upper right-hand side). O:1s Auger spectrum of TFIP-d_1 on a Si(100) surface. (a) KVV NAES. (b) KVVσ^* RAES.

Figure 3 (bottom). F:1s Auger spectrum of TFIP-d_1 on a Si(100) surface. (a) KVV NAES. (b) KVVσ^* RAES.

(BL2B1)

Site-Specific Fragmentation Following C:1s Core-Level Photoionization of $CF_3CD(OH)CH_3$ on a Si(100) Surface

Shin-ichi NAGAOKA, Arinobu NAKAMURA,[A] Shin-ichiro TANAKA[B] and Kazuhiko MASE[C]

Institute for Molecular Science, Okazaki 444-8585

[A]Department of Chemistry, Faculty of Science, Ehime University, Matsuyama 790-8577

[B]Department of Physics, Graduate School of Science, Nagoya University, Chikusa-ku, Nagoya 464-8602

[C]Photon Factory, Institute of Materials Structure Science, High Energy Accelerator Research Organization, 1-1 Oho, Tsukuba 305-0801

Synchrotron radiation has provided a powerful means to obtain information about core-level excitations, and the dynamic processes following the core-level excitations in molecules have long been a subject of interest. In contrast to valence electrons that are often delocalized over the entire molecule, the core electrons are localized near the atom of origin. Although core electrons do not participate in the chemical bonding, the energy of an atomic core-level in the molecule depends on the chemical environment around the atom. A shift in the energy levels of core electrons that is due to a specific chemical environment is called a chemical shift.

Monochromatized synchrotron radiation can excite core electrons of an atom in a specific chemical environment selectively, discriminating the core electrons from those of like atoms having different chemical environments. This site-specific excitation often results in site-specific fragmentation, which is of importance in understanding localization phenomena in chemical reactions and which is potentially useful for synthesizing materials through selective bond breaking. Synchrotron radiation can indeed play the part of an optical knife for molecules. When bond dissociation around an atomic site is required in the synthesis, one can use the optical knife that has the photon energy corresponding to the specific excitation of that site.

To elucidate the site-specific fragmentation, we have studied the spectroscopy and dynamics following core-level photoionization of various molecules condensed on surfaces [1-4]. In the present work, we have used the energy-selected-photoelectron photoion coincidence (ESPEPICO) method to study the site-specific fragmentation following C:1s photoionization of $CF_3CD(OH)CH_3$ (TFIP-d_1) on a Si(100) surface. Since the chemical environments of a C atom bonded to three F atoms (C[F]), of C bonded to three H atoms (C[H]) and of C bonded to an OH group (C[O]) are different from one another, TFIP shows occurrence of different chemical shifts [4]. Thus it seems likely that TFIP-d_1 will show site-specific fragmentation.

Figures 1a, b and c respectively show the ESPEPICO spectra obtained with emissions of the C[O]:1s, C[H]:1s and C[F]:1s electrons of TFIP-d_1 monolayer adsorbed on a Si(100) surface. Figures 2a-c show the corresponding spectra of TFIP-d_1 monolayer adsorbed on Si(100) and

annealed at room temperature. Figures 3a-c show the corresponding spectra of TFIP-d_1 multilayer condensed on Si(100). H^+ ion is predominantly desorbed coincidentally with the C[H]:1s and C[O]:1s electrons in Figures 2a and b. In contrast, F^+ ion is predominantly desorbed coincidentally with the C[F]:1s electron. Such site-specific fragmentation is not clearly revealed in Figures 1 and 3. Further investigations are clearly needed on the reason for this difference.

[1] S. Nagaoka, K. Mase, M. Nagasono, S. Tanaka, T. Urisu and J. Ohshita, J. Chem. Phys. **107**, 10751 (1997).

[2] S. Nagaoka, K. Mase and I. Koyano, Trends Chem. Phys. **6**, 1 (1997).

[3] S. Nagaoka, K. Mase, M. Nagasono, S. Tanaka, T. Urisu, J. Ohshita and U. Nagashima, Chem. Phys. **249**, 15 (1999).

[4] K. Mase, S. Tanaka, S. Nagaoka and T. Urisu, Surf. Sci. **451**, 143 (2000).

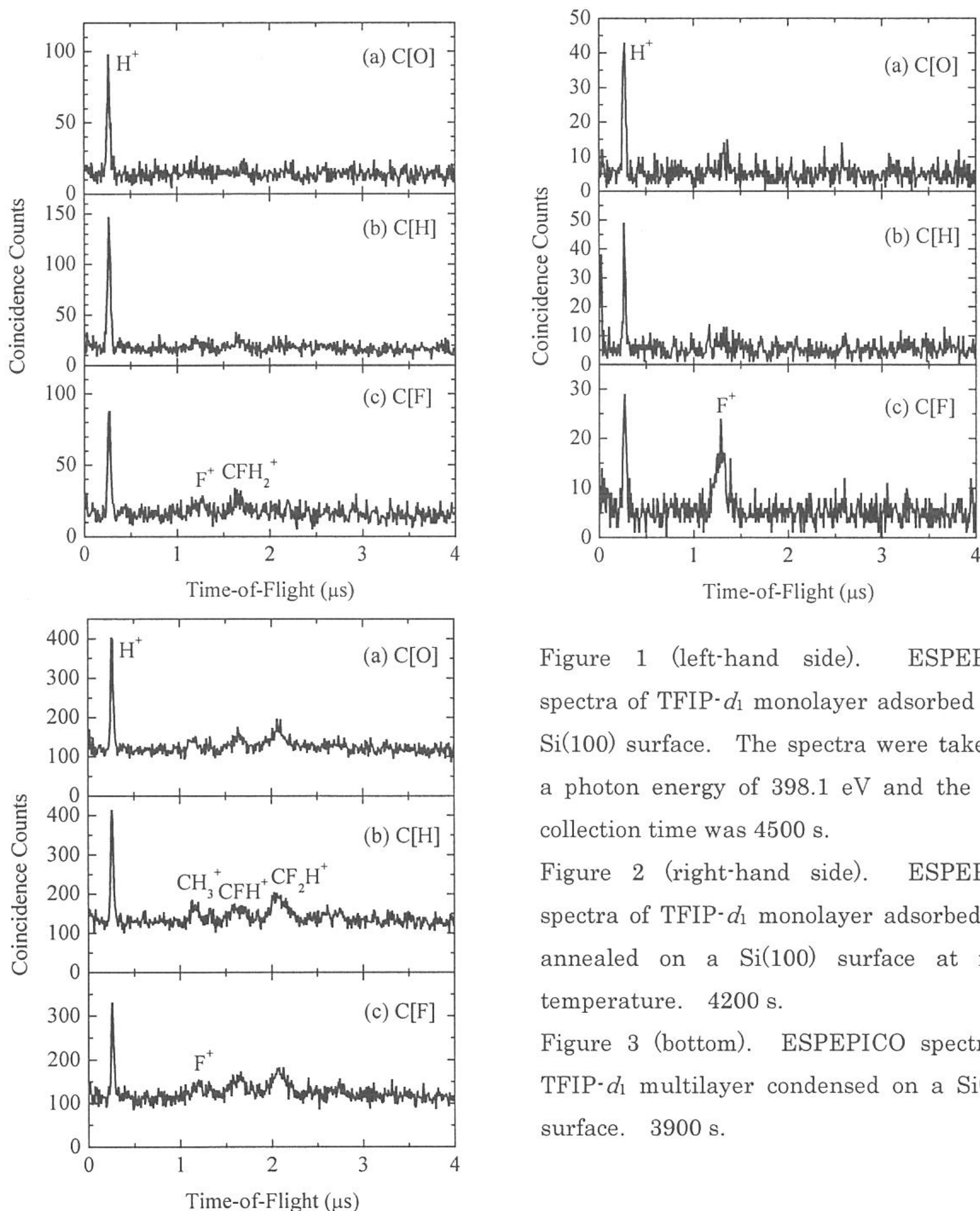

Figure 1 (left-hand side). ESPEPICO spectra of TFIP-d_1 monolayer adsorbed on a Si(100) surface. The spectra were taken at a photon energy of 398.1 eV and the data collection time was 4500 s.

Figure 2 (right-hand side). ESPEPICO spectra of TFIP-d_1 monolayer adsorbed and annealed on a Si(100) surface at room temperature. 4200 s.

Figure 3 (bottom). ESPEPICO spectra of TFIP-d_1 multilayer condensed on a Si(100) surface. 3900 s.

(2B1)

Observation of the surface states on the TiO_2(110) surface by using the photo-stimulated ion desorption.

S. Tanaka[1], S. Nagaoka[2] and K. Mase[3]

[1]Department of Physics, Graduate School of Science, Nagoya University, Furo-cho, Chikusa, Nagoya 464-8602, Japan
[2]Institute for Molecular Science, Myodaiji, Okazaki 444-8585, Japan
[3]Institute for Material Structure Science, Tsukuba 305-0801, Japan

Introduction A number of investigations have been carried out on the surface of the TiO_2, and a rutile (110) surface has been particularly studied by many authors. However, many things still remain unknown. For instance, intrinsic surface states of the rutile (110) surface have not yet experimentally observed although some theoretical calculations have predicted that they would have different binding energies. In this report, we measure the photo-stimulated desorption in order to observe the NEXAFS (Near edge X-ray absorption fine structure) of the rutile (110) surface, and detected the surface (unoccupied) states.

Experiments All experiments have been carried out at the BL2B1 of the UVSOR, IMS. Soft-X ray of photon energies near the Ti-$L_{2,3}$ and O-K thresholds were monochromized by a grasshopper monochromator, and injected to the rutile (110) surface. Ejected ions and electrons as functions of photon energies were detected by a home-made EICO (Electron-Ion Coincidence) apparatus which equipped with a CMA (Cylindrical Mirror Analyzer) for electrons and a TOF tube for ions. Coincidence measurements with electrons and ions were separately carried out in order to determine ion species. The rutile (110) surface was cleaned by Ar^+ sputtering and heating followed by annealing in oxygen (10^{-6} Torr). It was a nearly perfect surface, in which a number of oxygen vacancies was small as observed with the photoelectron spectroscopy.

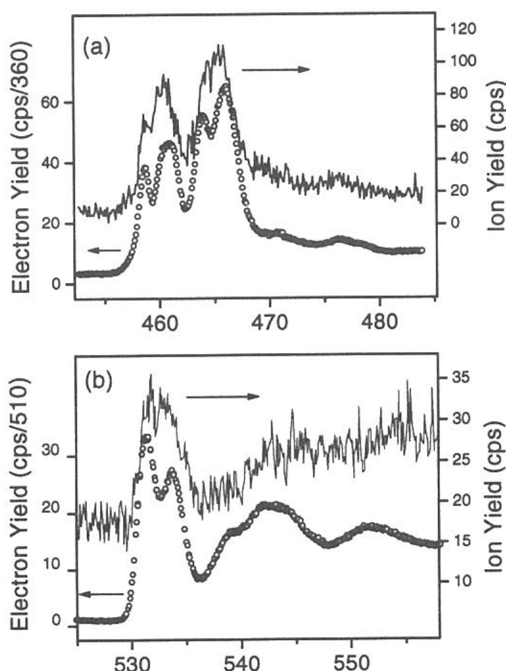

Figure 1

Results and Discussion Figure 1 shows electron (open circles) and ion (solid lines) yields near (a):Ti-$L_{2,3}$ and (b):O-Kedges. The electron yield predominantly represents the bulk absorption, and ion yield the surface absorption. In these spectra, desorbed ions were mostly O^+ according to the coincidence measurements. Here, we focus on near edge structures, because it is expected that they show electronic structures (density of states) of the unoccupied states. In figure 2, curves (a) and (b) show the ion yields and (c) and (d) show the electron yields, where the x axis represents the relative energies referred to the threshold at Ti-L_3 (a and c) and O-K (b and d) edges, which approximately indicates the binding energy of the unoccupied states from the Fermi level. Because the core electron is strongly localized, the absorption curve is expected to indicate the partial density of states at the atoms involving the core electron to participate the transition. Thus, the spectra at the O-K edges approximately show the O-2p contribution to the unoccupied levels, and those at the Ti-L_3 edges show the Ti-3d contribution. The density of states observed in fig. 2 for Ti-3d and O-2p are rather similar to each other both in electron (bulk sensitive) and ion (surface sensitive) yields. It indicates that the hybridization between the Ti-3d and O-2p is strong in the unoccupied states of the rutile,

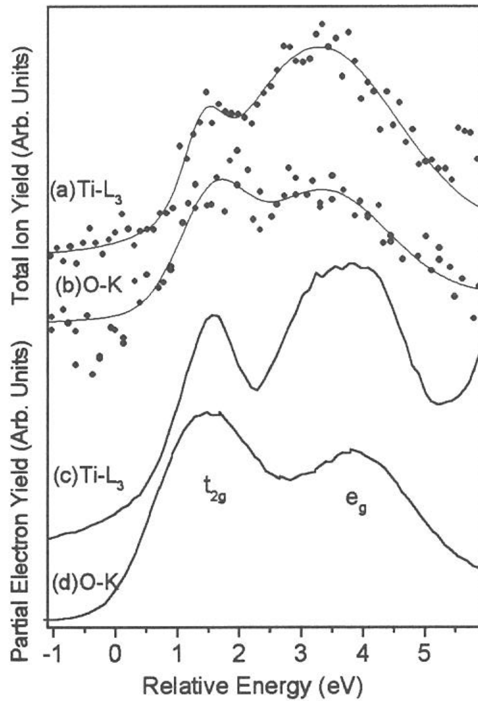

Figure 2

and rules out a simple picture that the rutile is an ionic crystal where O-2p is fully occupied and Ti-3d is fully empty. Ti-3d splits into t_{2g} and e_g levels due to the crystal field made by surrounding oxygen ions. It is interesting to point out that the e_{2g} energies observed in the ion yields is shifted by about 1 eV compared to the electron yield while the t_{2g} levels do not show such differences. It is known that the energy of e_g is more sensitive to the symmetry of the crystal field than that of the t_{2g}. Thus, it is reasonable to conclude the 1 eV shift is a bulk-to-surface shift in the binding energies of the e_g level at the rutile surface. This shift is consistent with the experimental work. This is the first observation of the intrinsic surface states on the rutile(110) surface to our knowledge.

(2B1)

Ion Desorption from H_2O/ZnO(1010) and H_2O/TiO_2(110) surfaces induced by the core-level excitation

S. Tanaka[1], S. Nagaoka[2] and K. Mase[3]

[1]Department of Physics, Graduate School of Science, Nagoya University, Furo-cho, Chikusa, Nagoya 464-8602, Japan

[2]Institute for Molecular Science, Myodaiji, Okazaki 444-8585, Japan

[3]Institute for Material Structure Science, Tsukuba 305-0801, Japan

Ion desorption from solid surfaces is one of the most fundamental processes in the photochemical reaction. In this report, a comparison in the hydrogen ion desorption from water-chemisorbed ZnO and TiO_2 surfaces will be presented, and a mechanisms of them will be discussed.

A nominal electronic configuration of ZnO is $(Zn3d)^{10}(O2p)^6$, and that of TiO_2 is $(Ti3d)^0(O2p)^6$. However, in both metal oxides, the hybridization among electrons in metal and oxygen atoms is considerably large. It is generally accepted that water dissociates on ZnO(1010) and TiO_2(110) surfaces and the OH species is bonded to the metal (Zn and Ti) atoms mainly at the oxygen vacant site according to previous studies.

We made photoelectron-photoion coincidence measurements on both surfaces. The experiments have been carried out at BL2B1 of UVSOR. The samples were cleaned by Ar^+ sputtering and annealing in UHV and oxygen ($1x10^{-6}$ Torr). Samples were heated to high temperature (about >900K) in UHV at the final stage of the cleaning to produce oxygen vacancies at the surfaces, then exposed to H_2O gas at room temperature.

Figure 1 shows a photoelectron and photoelectron-photoion coincidence spectra for the water-chemisorbed ZnO(1010) surface. The left-hand side shows a photoelectron spectrum and the right-hand side shows TOF spectra of ions to be triggered by the detection of photoelectrons whose kinetic energies are indicated by bars in the left-hand side. The photon energy used was 680 eV. Peaks observed in the photoelectron spectrum are ascribed to the oxygen

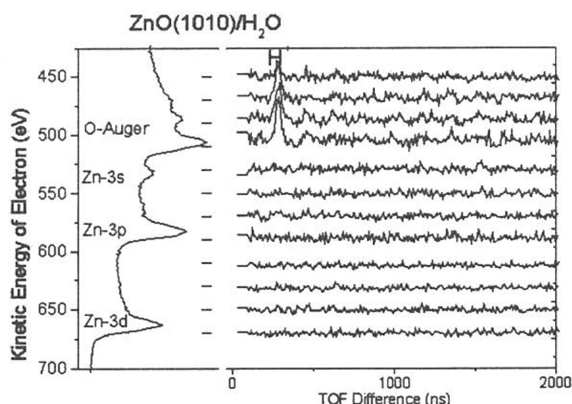

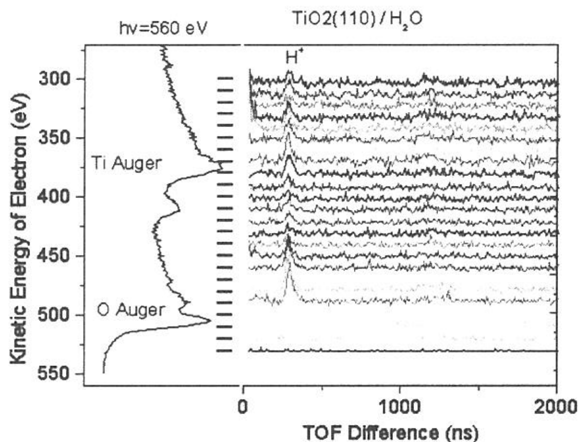

KVV Auger electron emission and the core-level photoelectron emission from Zn as shown in the figure. In the coincidence spectra, the desorption of H^+ is observed at the oxygen Auger electron emission, and no coincidence was observed with the electron emission from Zn. This indicates that the excitation and decay within the oxygen atom leads to the H^+ desorption from the OH species. Meanwhile, the excitation and decay at Zn, which is not bonded to H, dose not yield any ion desorption. A results for the water-chemisorbed $TiO_2(110)$ is drastically different from ZnO(1010). The H^+ desorption coincides not only with the electron emission from O, but also with that from Ti as shown in figure 2. Thus, in the case of the TiO_2, the excitation and decay at Ti, which is not directly bonded to H, can yield the H^+ desorption.

In the classical Knotek Feiblman model for TiO_2, the ion desorption is induced by holes at O2p created by the inter-atomic Auger decay of the Ti3p hole (which can be produced by the Auger decay of any Ti core levels deeper than Ti3p), because there are no higher levels than Ti3p except O2p. However, it seems to be difficult to explain the results shown above with that scenario, because 1) the valence band of TiO_2 is strongly hybridized, and the decay of the Ti core levels without any inter-atomic Auger process is possible and 2) Zn3d level is the highest level at Zn which is below the O2p level, so, similar mechanism might be expected in ZnO as well as TiO_2. Thus, it is necessary to find another mechanism. It is reasonable to assume that the mechanism of the ion desorption induced by the Ti-core level excitation should be related to a presence of the empty Ti3d level in TiO_2, because this is the most significant difference between TiO_2 and ZnO. We propose a model in which the charge transfer from O2p to Ti3d through the hybridization induced by the Ti3p core hole potential (similar to the Kotani-Toyozawa model in the photoelectron spectroscopy) is responsible for the charge transfer from O to Ti and also for the ion desorption. This model is consistent with the experimental result shown above because the process is inhibited in ZnO because Zn3d is not empty.

(BL2B1)

Adsorption, Desorption And Dissociation of Nitrous Oxide over Palladium (110) at Low Temperatures

H. Horino,[a] S. Wako,[a] T. Matsushima,[b] S. Nagaoka,[c] E. Nakamura,[c] S. Tanaka[d] and M. Kamada[c]

[a] *Graduate School of Environmental Earth Science, Hokkaido University, Sapporo 060-0810, Japan*
[b] *Catalysis Research Center, Hokkaido University, Sapporo 060-0811, Japan*
[c] *Institute for Molecular Science, Myodaiji Okazaki 444-8585, Japan*
[d] *Department of Physics, Nagoya University, Senju, Nagoya 464-0814, Japan*

Catalytic N_2O decomposition on metal surfaces has attracted much attention because N_2O is harmful, yielding a remarkable greenhouse effect, and is also a by-product in catalytic NO decomposition. In the latter, this species was recently identified as the intermediate emitting N_2 on Pd(110)[1]. N_2O decomposition depends strongly on the kind of metals and also their surface structures. Desorption of N_2O(a) is completed without dissociation at 90-120 K on Pt(111), Ir(111), Ni(111) and Ag(111). On the other hand, N_2O(a) dissociates at around 100 K on Ru(001) and W(110). This abstract delivers the first report of NEXAFS data of N_2O on Pd(110), showing a molecular adsorption state, and also of decomposition on this surface at low temperatures, showing four N_2 desorption peaks with different angular distributions.

Experimental

[Near-edge X-ray absorption fine-structure] The angle of X-ray incidence (χ) with respect to the surface normal was varied by rotating a Pd(110) crystal such that the electric vector of the X-ray, ***E***, was oriented in a plane parallel to or perpendicular to the $[1\bar{1}0]$ direction. The crystal was kept below 70 K during the NEXAFS measurements. The NEXAFS spectra were recorded by an Auger electron yield mode with the kinetic energy of the nitrogen KLL Auger electrons at 382 eV [2].

[Angle-resolved thermal desorption] A UHV system with three chambers was used. The reaction chamber was equipped with LEED-AES, an Ar+ gun, and a mass spectrometer for angle-integrated (AI) analysis [3]. The collimator had a slit on each end and the analyzer had another mass spectrometer for angle-resolved (AR) measurements. The crystal was set on the top of a rotatable manipulator to change the desorption angle (θ ;polar angle). This angle was scanned in a plane along the [001] direction because N_2 desorption was concentrated in this plane. The surface after flashing to 1100 K was exposed to $^{15}N_2O$ through a gas doser when the surface temperature (T_S) was below 95 K. Hereafter, isotope ^{15}N is designated as N.

Results and Discussion

[NEXAFS] On a clean surface, no signal peaks were found in raw NEXAFS spectra in the photon energy range from 395 eV to 430 eV. On the other hand, two resonance states were clearly seen in NEXAFS spectra at 403.2±0.5 and 406.7±0.5 eV when the surface was exposed N_2O at 70 K (Fig. 1). The former was assigned to the transition from the 1S state of the terminal nitrogen atom to 3 π *, and the latter due to the excitation of a 1S electron of the center nitrogen to 3 π *. This energy difference of 3.3 eV agrees well with the results on Ni(111) and confirms the molecular form of N_2O.

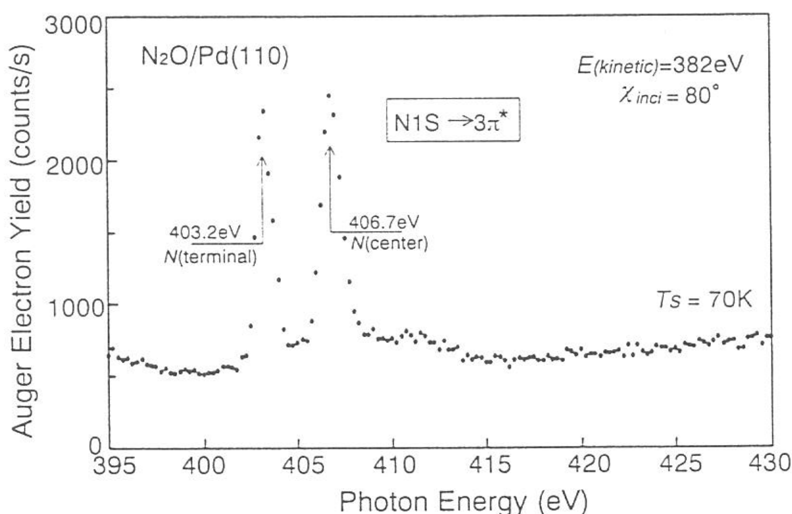

Fig. 1 NEXAFS spectra of N_2O ad-molecules at an incidence angle (χ) of 80 °
The electric vector ***E*** was in a plane along the [001] direction.

[AR-TDS] $N_2O(a)$ is mostly decomposed during heating procedures, emitting N_2 (g) and leaving O(a). N_2 showed four desorption peaks, β_1-N_2 at 140-160 K, β_2-N_2 at 132-138 K, β_3-N_2 at 123-127 K and β_4-N_2 at 105-111 K (Fig. 2a)[4]. The first was found at high N_2O exposures and the last at very low exposures. Both β_1-N_2 and β_3-N_2 revealed sharp and inclined emission collimated at θ =43° off the surface normal in the (001) plane, β_4-N_2 sharply collimated around θ =55° , and β_2-N_2 showed a cosine form below half saturation. The total amount of emitted N_2 showed a good linearity with increasing N_2O exposure and a passing at the origin of the exposure curve, indicating that N_2O including the product of N_2 is trapped on the surface at 95 K. No removal of product N_2 was noticed during exposure at 95 K.

The AR signal of N_2 showed different peak shapes as shown in Fig. 2b. The β_4-N_2 peak became clear at Θ_{N2O}=0.03 and around θ =50°, where Θ_{N2O} is the relative coverage of N_2O normalized to the desorption maximum of N_2 and N_2O. It is maximized at around θ = +55° and -55° in the (001) plane, as approximated by $\cos^{40}(\theta+55) + \cos^{40}(\theta-55)$. At this coverage, the β_3-N_2 was not significant. The β_2-N_2 peak in AI form was higher than the others, however, its intensity in AR form was lower than the others. The value at θ = 90° remained about 60 % of that at θ = 0°. This remaining signal is due to N_2 molecules that did not pass through the slits directly from the surface, but were first desorbed into the reaction chamber and penetrated from there into the analyzer. This extraneous signal was subtracted from the observed AR signal at θ <90° when the signal was plotted against θ. The resultant β_2-N_2 showed a simple cosine distribution.

At high Θ_{N2O} values, β_3-N_2 was enhanced especially around θ =43°, whereas β_4-N_2 was relatively suppressed and β_2-N_2 increased. β_3-N_2 sharply peaked at around θ = +43° and -43° in the [001] plane, as represented by $\cos^{51}(\theta+43) + \cos^{51}(\theta-43)$ (Fig. 2c). β_1-N_2 was sensitive to θ at around θ =43°. It showed a sharp collimation at around ±43° off the surface normal direction. On the other hand, β_2-N_2 became sensitive to θ at around ±43° at high exposures. This is probably due to the contribution from enhanced β_1-N_2 and β_3-N_2.

[Inclined desorption] Prior to decomposition, $N_2O(a)$ must lie on the surface because oxygen is released on it. A simple dissociation of inclined N_2O bonding to metal through the O-end may emit N_2 into an inclined way, although such configuration has not been confirmed by vibrational spectroscopy. In N_2O dissociation, a surface parallel momentum can be transferred to nascent N_2 from the other product oxygen atom immediately after N_2O dissociation, because a high energy (about 2 eV) is released in the subsequent formation of O-metal bond.

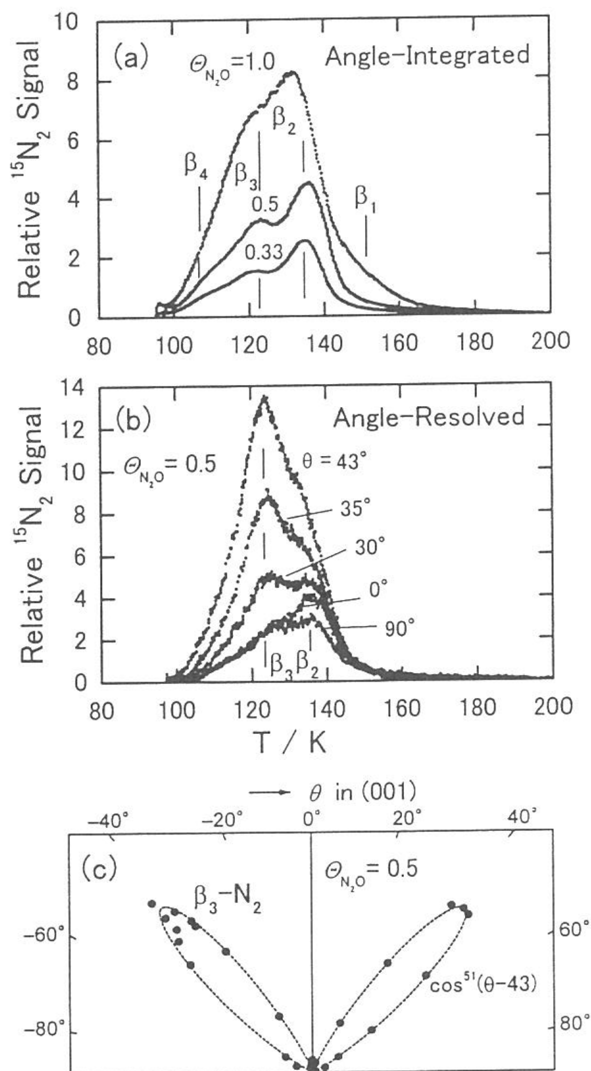

Fig. 2 TDS spectra of N_2 from N_2O-covered Pd(110) in (a) angle-integrated and (b) angle-resolved forms at different θ values in the (001) plane. The heating rate was 0.4 K/s. (c) Angular distribution of desorbing β_3-N_2 in the (001) plane at Θ_{N2O} = 0.5.

Reference

1. I. Kobal, K. Kimura, Y. Ohno, H. Horino,I. Rzeznicka, T. Matsushima, Stud. Surf. Sci. and Catal. 130 (2000) 1337-1342.

2. S. Wako, M. Sano, Y. Ohno, T. Matsushima, S. Tanaka, M. Kamada, Surf. Sci. 461 (2000) L537-542.

3. I. Rzeznicka, Y. Ohno, H. Horino, I. Kobal, K. Kimura, T. Matsushima, Hetero. Catal. Proc. 9th Intern. Symp. Eds. L. Petrov, Ch. Bonev, G. Kadinov, (2000) page 97-102.

4. H. Horino, S. Liu, M. Sano, S. Wako, Y. Ohno, A. Hiratsuka, T. Matsushima, Topics in Catal. in press (2001) .

(BL3A-1)

Investigation of Photo-dissociation Process of Organo-metallic Compounds : TEOS($Si(OC_2H_5)_4$) and TEOG($Ge(OC_2H_5)_4$)

Yasuhiro Kawasaki, Hideaki Yanagida, Kou Kurosawa, Eiken Nakamura and Masao Kamada

Department of Electrical and Electronic Engineering, Miyazaki University

Institute for Molecular Science, Okazaki, 444-8585

SiO_2 and GeO_2 thin films have been prepared by photo-chemical vapor deposition (Photo-CVD) at room temperature from organo-metallic compounds: $Si(OC_2H_5)_4$ and $Ge(OC_2H_5)_4$, The photo-dissociation processes have not been clear yet. In this work, we have identified species dissociated from $Si(OC_2H_5)_4$ and $Ge(OC_2H_5)_4$ molecules by vacuum ultraviolet radiation and discussed about the photo-dissociation processes. The chemical structures are illustrated in Fig.1

TEOS and TEOG were supplied at 3.0×10^{-7} Torr and 7.0×10^{-6} Torr into a stainless steel pipe, respectively. The 10.7 eV photon beam was introduced into the pipe, which was provided by adjusting the undulator gap to be 35mm. The average photon density was 8.0×10^{13}photon/cm^2/100mA/sec.

The mass spectra taken from TEOS and TEOG before-radiation and during-radiation are shown Figs.3(a) and (b) and Fig.4(a) and (b), respectively. Our main aim of this study is to identify the final products associated with Si and Ge photo-dissociated from these molecules, so that we focus on the spectra at 28 (Si), 44 (SiO), 60 (SiO2), and 76 (SiO4) for TEOS, and 72(Ge), 88(GeO), 104 (GeO2), 120 (GeO3), and 136 (GeO4) for TEOG. By comparing the spectra from TEOS and TEOG, we can conclude that SiO and Ge are the main final products. In case of TEOS, a small amount of Si are produced. Taking into

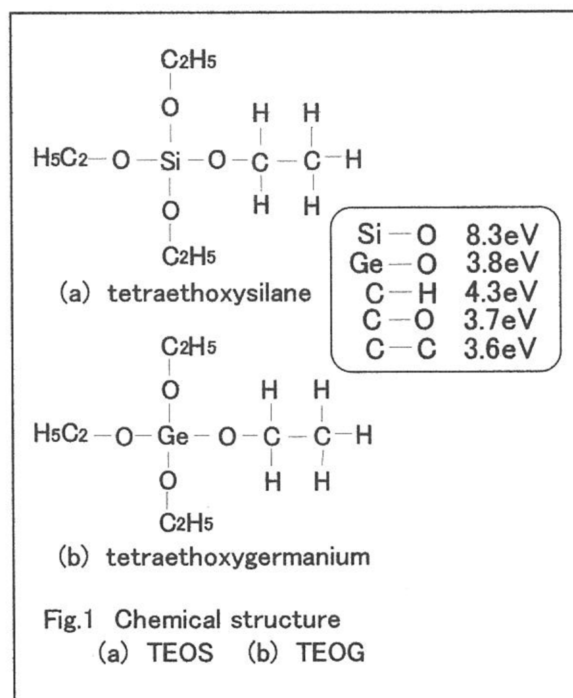

Fig.1 Chemical structure
(a) TEOS (b) TEOG

account of a fact that the bonding energies of Si-O and Ge-O are 8.3 eV and 6.9 eV, respectively, the difference induces the different final products.

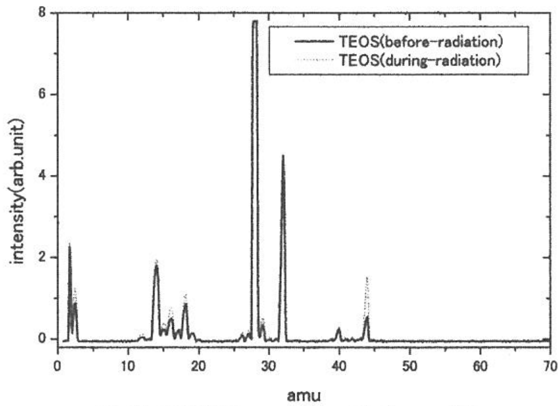

Fig.3(a) TEOS Mass spectra of before-radiation and during-radiation (m/e=1-70)

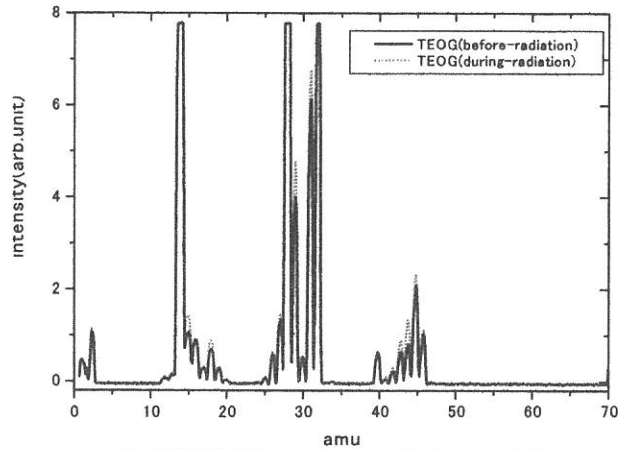

Fig.4(a) TEOG Mass spectra of before-radiation and during-radiation (m/e=1-70)

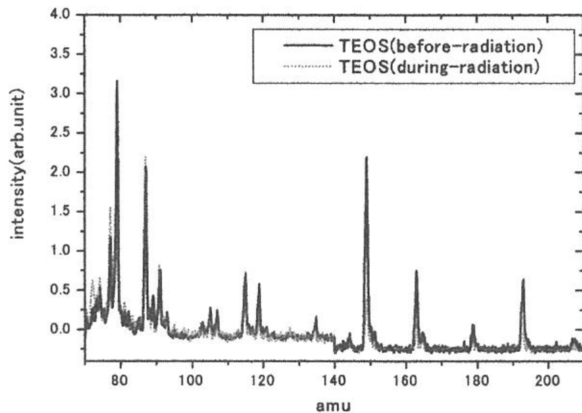

Fig.3(b) TEOG Mass spectra of before-radiation and during-radiation (70-210)

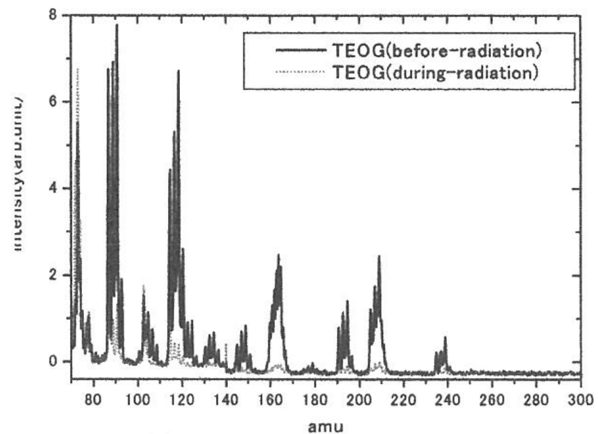

Fig.4(b) TEOG Mass spectra of before-radiation and during-radiation (m/e=70-300)

(BL4A)

Assignments of bending and stretching vibrational spectra and mechanisms of thermal decomposition of SiH_2 on Si(100) surfaces

Hideyuki Noda[a], Tsuneo Urisu[b]

[a]*The Graduate University for Advanced Studies, Myodaiji, Okazaki, 444-8585*
[b]*Institute for Molecular Science, Myodaiji, Okazaki, 444-8585*

Infrared (IR) absorption spectroscopy has contributed to identification of the chemical species on the hydrogen-adsorbed Si surface (H/Si) and elucidation of their structures. Despite extensive IR studies of H/Si systems, however, many fundamental problems in the assignment of vibrational modes and thermal reaction mechanisms remain unsettled. Even in the stretching vibrational region, reported assignments are still inconsistent. Most previous IR studies of H/Si surfaces have used the technique of attenuated total reflection (ATR), which can only provide spectra above about 1400 cm^{-1} because of Si lattice absorption. Buried metal layer-infrared reflection absorption spectroscopy (BML-IRRAS) has an advantage in that it supplies spectra with high sensitivity and high resolution (0.5-2 cm^{-1}) for the SiH_n bending and wagging vibrations, which appear in the so-called fingerprint region, <1000 cm^{-1} as well as the SiH_n stretching vibration. In this work, we have assignned the SiH_2 modes in the stretching and bending regions consistently by analyzing the temperature dependence of this spectrum and discussed mechanisms of the thermal decomposition of SiH_2 species.

Figure 1 shows typical BML-IRRAS spectra obtained after 500 L hydrogen exposure at different temperatures. The RHEED patterns were 1x1 for the sample exposed at 300 K and 3x1 for that exposed at 400 K. The spectra shown in Figs. 1(a) and (b) consist of the stretching and bending modes near 2100 and 900 cm^{-1}, respectively. The peak-resolved spectra for these vibrations, calculated assuming that the shape of each peak is Lorentzian, are also shown in Fig. 1. The stretching part is resolved to at least four clear peaks at 2082, 2100, 2107, and 2138 cm^{-1}. Assignments of the 2100 cm^{-1} peak are made with reference to these works to the symmetric stretching mode of coupled monohydride (M_{ss}), the broad peaks at 2138 and 2130 cm^{-1} to the SiH_3 stretching modes (T_s) and the 860 cm^{-1} peak to the SiH_3 symmetric deformation (T_{sd}) mode. The assignments of the 860 and 2138 cm^{-1} peaks to the SiH_3 species are also supported by their clear intensity decrease by the change from 1x1 to 3x1.

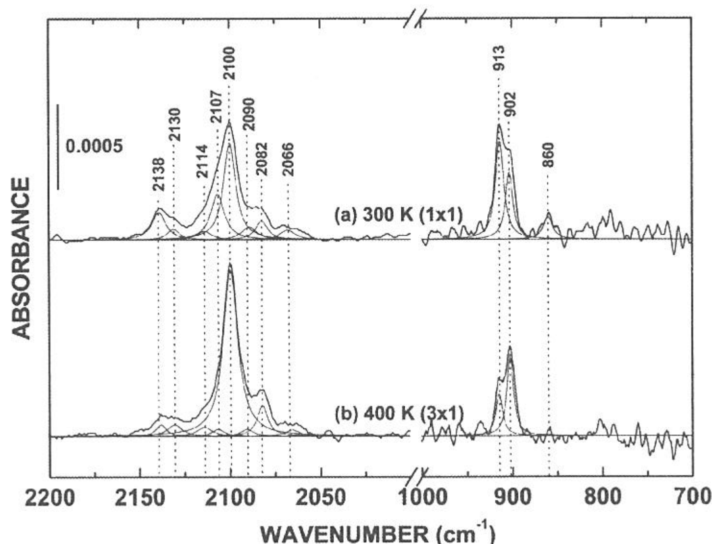

Fig. 1. p-Polarized BML-IRRAS spectra associated with H/Si(100) surfaces with (a) 1x1 (b) 3x1. Narrow lines show peak-resolved spectra calculated assuming that the the shape of each peak is Lorentzian.

As for the dihydride species, in previous reports, the weak peak at 2091 cm^{-1} was assigned to the SiH_2 symmetric stretching (D_{ss}), the 2114 cm^{-1} peak to the D_{ss} and the 2108 cm^{-1} peak for the HF-treated Si(100) surfaces to the D_{ss} of SiH_2 perpendicular to the Si(100) plane.

Of particular interest is the doublet peak in the bending vibration region that splits into two distinct peaks at 902 and 913 cm^{-1}. The IR absorption spectra of hydrogenated

porous silicon and the Si_2H_6 gas suggest that this doublet peak is a result of the SiH_2 bend scissors mode (D_{sci}) overlapping the degenerate deformation mode of SiH_3 (T_{dd}). McGonigal et al. assigned the small peak at 930 cm^{-1} to the T_{dd} and the strong peak at 860 cm^{-1} to the T_{sd} in their BML-IRRAS study of H on the polycrystalline Si surface. Since IR data with Si_2H_6 adsorbed porous Si and ab initio calculations imply that T_{dd} is much weaker (1/3 to 1/5) than that of the T_{sd} observed at 860 cm^{-1}, the SiH_3 bending mode, T_{dd}, should be weaker than the observable level in the present case. Moreover, the 907 cm^{-1} peak observed in a recent high-resolution (13 cm^{-1}) EELS study of H/Si(100) surfaces was assigned to the D_{sci} of the terrace dihydride and the small peak at 933 cm^{-1} to the T_{dd}. Therefore, we conclude that the 902 and 913 cm^{-1} peaks observed in the present work should both be assigned to D_{sci}. Furthermore, given the structures of 3x1 and 1x1 surfaces, we believe that there is adjacent dihydride (*AD*: H-Si-H H-Si-H), in addition to isolated dihydride (*ID*: H-Si-Si-H H-Si-H H-Si-Si-H), on the 1x1 surface that includes many phase boundaries of the 3x1 structures. It is also known that the vibrational frequencies of adsorbates on a solid surface are easily influenced by the neighboring species. In the IR absorption spectra of a-Si:H, the observed D_{sci} of the polysilane-like chain segment $(SiH_2)_n$ is about 10 cm^{-1} higher than that of the normal SiH_2. We therefore assign the 902 cm^{-1} peak in Fig. 1 to the bend scissors mode of *ID* (ID_{sci}), and that the 913 cm^{-1} peak to the same mode of *AD* (AD_{sci}). These assignments are also supported by that the 913 cm^{-1} peak is weaker for the 3x1 structure (Fig. 1(b)) than that for the 1x1 structure (Fig. 1(a)).

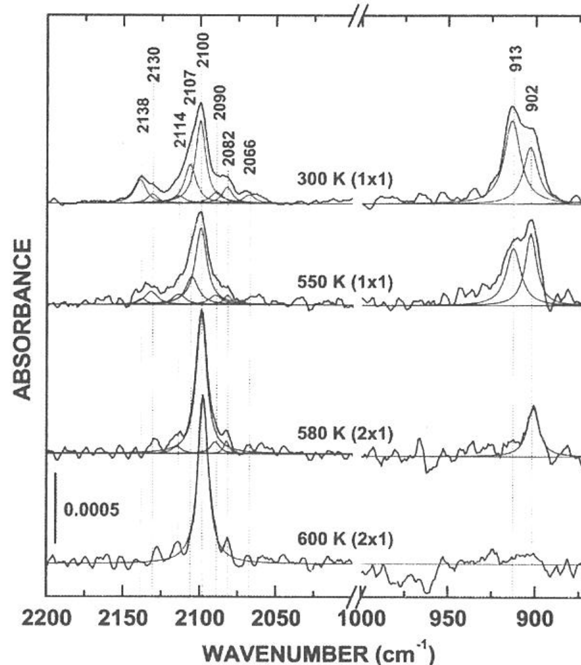

Fig. 2. BML-IRRAS spectra obtained at various annealing temperatures. Narrow lines show peak-resolved spectra calculated assuming that the the shape of each peak is Lorentzian.

To confirm the assignments of the SiH_2 species, we investigated the dependence of this peak intensity for the 1x1 surface on the annealing temperature (Fig. 2). The IA of the 2100 cm^{-1} peak starts to increase at about 500 K and that of the 913 cm^{-1} peak starts to decrease at nearly the same temperature. As shown in Fig. 2, the temperature dependence of the 913 cm^{-1} peak almost coincides with that of the 2107 cm^{-1} peak. We therefore assign the 2107 cm^{-1} peak to the symmetric stretching mode of *AD* (AD_{ss}). It is difficult to account for the temperature dependence of the two peaks at 2090 and 2114 cm^{-1} in detail from the data shown in Fig. 2, but both peaks are found in the spectra of samples annealed up to 550 or 580 K, in contrast to those of samples annealed at higher temperatures. Both peaks are therefore assigned to the vibrational modes of the dihydride species. Furthermore, because the temperature dependence of the 2090 cm^{-1} peak shown in Fig. 2 is similar to that of the 902 cm^{-1} peak, we assign the former peak to the symmetric stretching mode of *ID* (ID_{ss}), as reported by Chabal et al. On the other hand, Dumas et al. assigned the 2114 cm^{-1} peak observed in their IR study of the HF-treated Si(100) surface to the asymmetric stretching of the tilted dihydride ("horizontal" dihydride on the (111) facets) on an atomically rough H-terminated Si(100) surface; we therefore assign the small peak at 2114 cm^{-1} to the SiH_2 asymmetric stretching mode (D_{as}) on defect sites.

From the annealing temperature dependence shown in Fig. 2, we conclude that *AD* is slightly less stable than *ID* and that both *AD* and *ID* produce coupled monohydride by thermal decomposition. *AD* can easily generate coupled monohydride by thermal decomposition via second-order kinetics, the thermal reaction of *ID* may generate coupled monohydride by the decomposition reaction accompanied by the rearrangement of hydrogen.

(BL4A)

Initial Stage of Hydrogen Etching of Si Surfaces Investigated by Infrared Reflection Absorption Spectroscopy

Hideyuki Noda[a], Tsuneo Urisu[b]

[a]*The Graduate University for Advanced Studies, Myodaiji, Okazaki, 444-8585*
[b]*Institute for Molecular Science, Myodaiji, Okazaki, 444-8585*

Hydrogen-adsorbed Si (H/Si) surfaces have attracted considerable interest in the fields of semiconductor technologies, because H plays important roles in the passivation effect and in several chemical-vapor-deposition reactions on the Si surface. Recently, some studies by temperature-programmed-desorption (TPD) and scanning tunneling microscopy (STM) have also shown the evidence of etching reactions involving by H atoms adsorbed on Si surfaces. This indicates that H atoms break Si back bonds and remove the Si atom from the surface. Clarifying the H-etching process will be significant in future nanoprocesses including atom-level control. In this work, we have investigated the initial stage of etching reaction of Si(100) and Si(111) surfaces induced by H-exposure using buried metal layer-infrared reflection absorption spectroscopy (BML-IRRAS).

Figure 1 shows IRRAS spectra of H/Si(100) surface formed at room temperature (RT) as a function of H-exposure. The three peaks at 902, 913 and 860 cm^{-1} in the bending part have been assigned to the isolated SiH_2 scissors (ID_{sci}), adjacent SiH_2 scissors (AD_{sci}) and SiH_3 symmetric deformation (T_{sd}) modes, respectively. The detection of the T_{sd} peak indicates that the initial stage of H-etching (breaking of the Si-Si back bonds) is occuring and that trihydride is forming. The H-exposure dependence of the integrated absorbance of these bending vibrations, calculated assuming the shape of Lorenzian, are plotted in Fig. 2. As shown in Figs. 1 and 2, the ID_{sci} peak appears and saturates at relatively low H-exposures (50 L). On the other hand, the AD_{sci} peak becomes clear at around 100 L and tends to saturate at 200-500 L. We can see that the T_{sd} appears and begins to increase gradually at the same time when the AD_{sci} almost saturates above 200 L. This means that the adjacent SiH_2 structure is a precusor to the SiH_3 formation.

Figure 3 shows a series of IRRAS spectra of H/Si(111) surface obtained by H-exposures at RT. At low exposures (~10 L), adatom monohydride (M'_s), observed at 2074 cm^{-1} is mainly formed on the surface. With increasing exposures (~30 L), the intensity of the M'_s peak decreases and the 905 cm^{-1} peak (D_{sci}) appears. This means that one back bond of Si adatom is broken, and that the adatom dihydride forms. As the exposure increases above 70 L, the 860 cm^{-1} peak (T_{sd}), which indicates the formation of adatom trihydride, increase gradually and saturates at 500 L. The formation of adatom higher hidrides by breaking of the adatom back bonds enlarges the H-terminated 1x1 area. Therefore, the 2080 cm^{-1} peak (M_s) increases remarkably as the exposure increases from 500 to 2000 L. Figure 4 shows IRRAS spectra of H/Si(111) surface obtained at RT by much higher

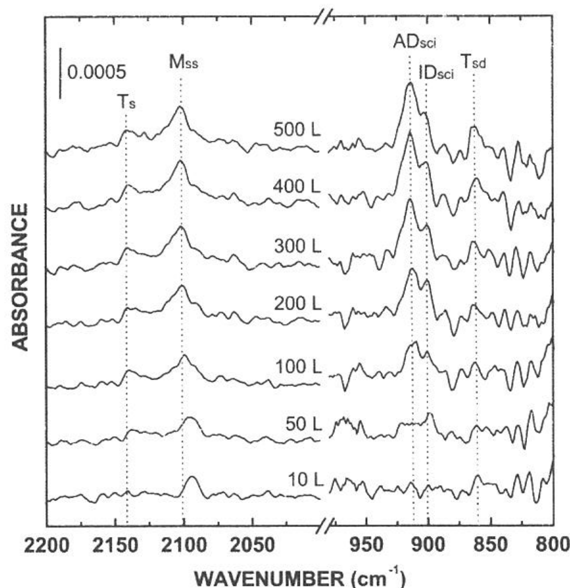

Fig. 1. BML-IRRAS spectra of p-polarization for H/Si(100) formed by H-exposure at RT.

H-exposure of 5000, 10000 and 50000 L. The most important result is that the SiH_3 symmetric deformation vibration peak (T_{dd}: 940 cm^{-1}) is observed at above 10000 L. Appearance of the T_{dd} peak means that the initial stage of etching of the 1x1 rest-atom layer occurs and the tilted trihydrides are formed. As for the adatom trihydride of which the symmetry axis is perpendicular to the surface, p-polarized IR beam excite the T_{sd} mode but not the T_{dd} mode. On the other hand, as for the trihydride formed by the etching of the 1x1 terrace having tilted symmetry axis against the (111) direction, both peaks of T_{dd} and T_{sd} are observable. The etching of the 1x1 terrace is also supported by the distinct decrease and broadening of the M_s peak indicating the increase of the surface roughness.

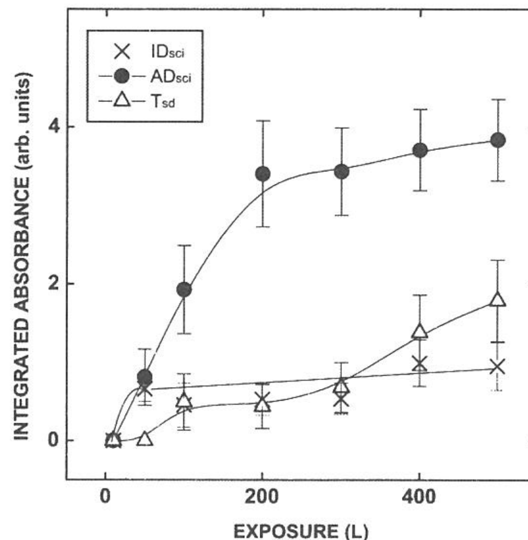

Fig. 2. Dependence on H-exposure of the integrated absorbances for the ID_{sci}, AD_{sci} and T_{sd} peaks in the Fig. 1 spectra.

Initial stage of etching reactions on Si(100) and Si(111) surfaces, induced by H-exposure at RT, has been investigated by BML-IRRAS. The SiH_2 scissors and SiH_3 deformation modes have been observed as clear indicators at the initial stage of etching reactions. On the Si(100) surface, the etching reaction started in the relatively low exposure region of ≥300 L. We found that the adjacent dihydride is a precursor structure of breaking the Si back bonds. On the Si(111) surface, adatom's back bonds were easily broken at a low H-exposure of 30-500 L. Adding to this dominant reaction, the etching of rest-atom layer was observed at higher H-exposures than 10000 L.

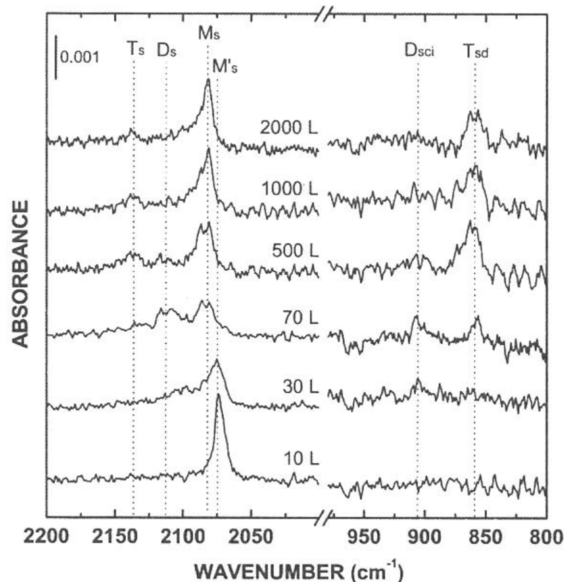

Fig. 3. BML-IRRAS spectra of p-polarization for H/Si(111) formed by H-exposure at RT.

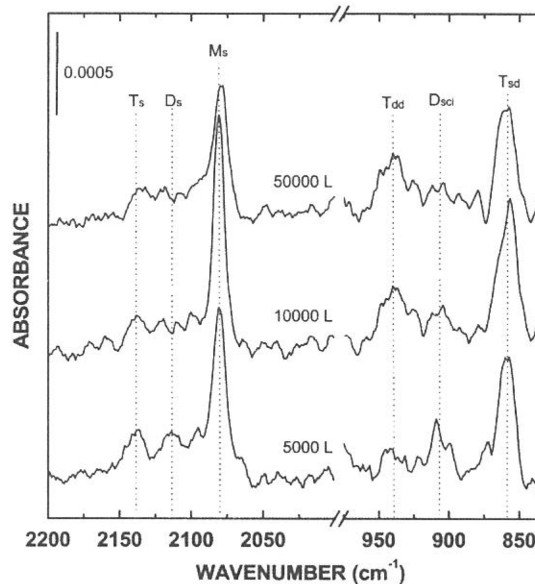

Fig. 4. BML-IRRAS spectra of p-polarization for H/Si(111) formed by high H-exposure of 5000, 10000 and 50000 L.

(BL-4A1)

X-ray lithography of PMMA sheets using white beam of the beam line BL4A1

Harutaka Mekaru[a], Yuichi Utsumi[a], Tadashi Hattori[a], and Tsuneo Urisu[b]

[a]*Laboratory of Advanced Science and Technology for Industry, Himeji Institute of Technology, koto, kamigorii, Ako, 678-1205*

[b]*Institute for Molecular Science, Myodaiji, Okazaki, 444-8585*

LIGA process, that utilizes a useful industrial application of SR, is one of the promising technologies for fabrication of extremely tall three-dimensional microstructures with a large aspect ratio. This process was invented at the Institut Fur Mikrostrukturtechnik (IMT) of the Karlstuhe Nuclear Center (KfK) in 1980 [1]. Microstructures with height of over a few hundreds μm have been widely applied to various fields such as micro-mechanics, micro-optics, sensor and actuator technologies, and chemical, medical and biological engineering.

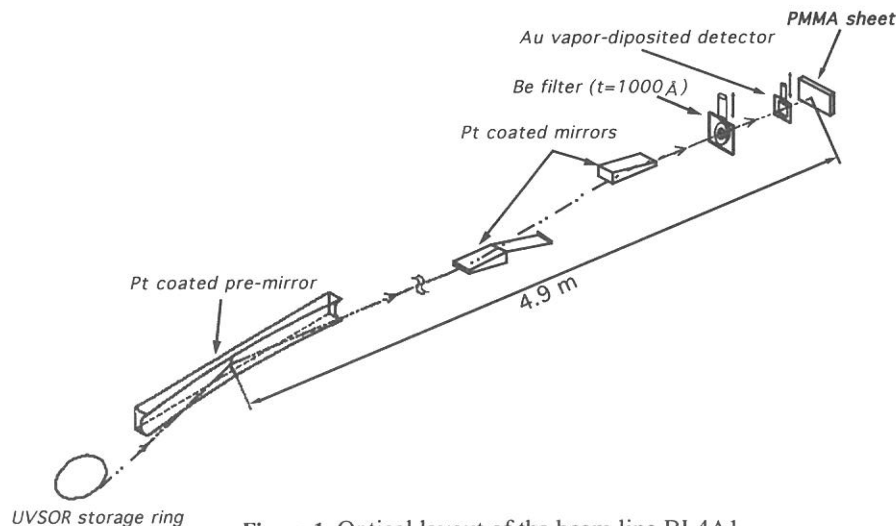

Figure 1. Optical layout of the beam line BL4A1

An X-ray deep lithography of the LIGA process needs the photon energies of 2 keV to 6 keV. The depth to which X-rays penetrate a resist depends on the resist's absorption coefficient for X-rays. The vacuum ultraviolet (VUV) photons contained in the SR can excite almost all electronic states, including core electrons. However, the penetration depth for PMMA in the photon energy range of the VUV has never been examined. This report is intended as an investigation of the X-ray lithography in the photon energy range less than 2 keV.

Figure 1 shows optical layout of a beam line BL4A1 in the UVSOR. The multilayered-mirror (MLM) monochromator beam line had been constructed specially for SR stimulated process. When the MLM is not used, the SR beam is reflected by a pair of Pt coated plane mirrors with grazing incident angles of 2 degrees in the white beam chamber

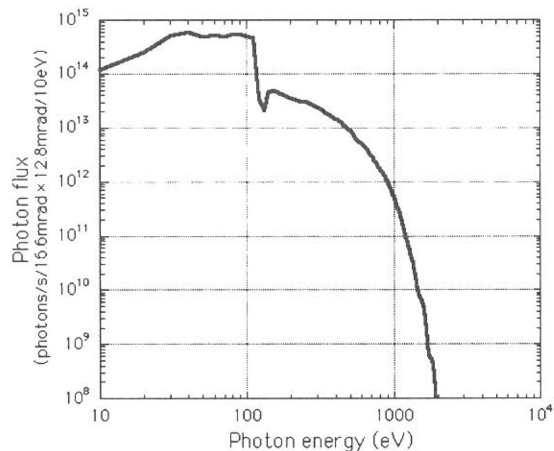

Figure 2. Calculated spectra of the photon flux of white beam in the beam lines BL4A1 of the UVSOR.

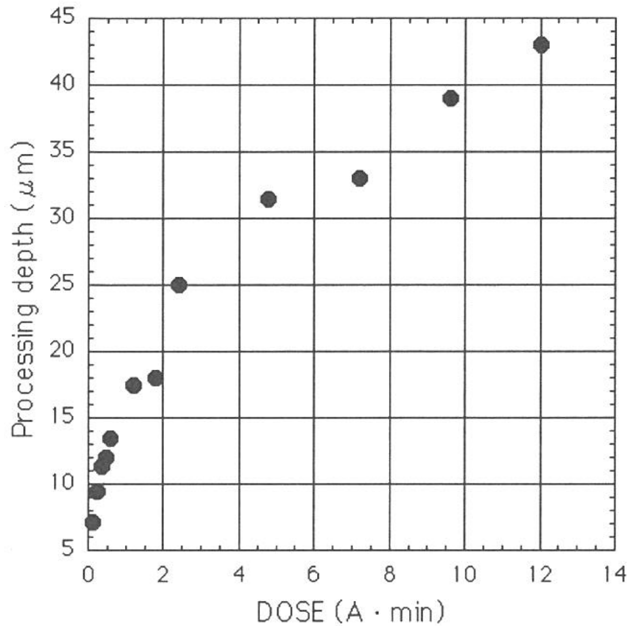

Figure 3. The dose dependence of PMMA sheet processing depth using the beam line BL4A1 of the UVSOR.

to keep the output beam at the same height as that of the output beam from the MLM monochromator. A Be filter is set to cut off low-energy photons, and an Au vapor-deposited detector is set to measure photo-current.[2], [3]

Figure 2 shows calculated the photon flux of the output beam at a point downstream of the exposure stage as a function of photon energy taking into consideration the acceptance angles and reflectivity of the pre-mirror, the reflectivity of two Pt-coted mirrors, and the transmission of the Be filter. The transmission (84%) of the mesh holding the thin Be film was also considered in addition to the transmission of the 0.1-μm-thick Be filter. The values of the optical constants used in the calculation were cited from reference 4.

As a fundamental data to estimate the required X-ray dose energy to process the required depth, the dependencies of processing depth and irradiated X-ray energy without any X-ray mask are measured. The processing depths after SR exposure and development were estimated maximum depths measured by the surface profiler (Dektak^3 ST). As shown in Fig. 3, processing depth increased linearly at low doses, while at high exposure doses it showed to gradually becoming saturation. The etching rate is estimated lower than that of the hard X-ray lithography in the photon energy range more than 1 keV. Furthermore, at the exposure doses more than 1.8 A• min, PMMA sheets become degenerating by thermal.

Finally, a patterning of the PMMA sheet was demonstrated by using the output beam with an Au wire mesh. The output beam irradiated on a 0.5 mm-thick PMMA sheet with an Au wire mesh at an exposure dose of 3.6 A• min. The diameter of the Au wire is 70 μm. Figure 4 shows the SEM image of PMMA microstructures. The patterning of the PMMA sheet was successfully demonstrated by using the output beam of the beam line BL4A1.

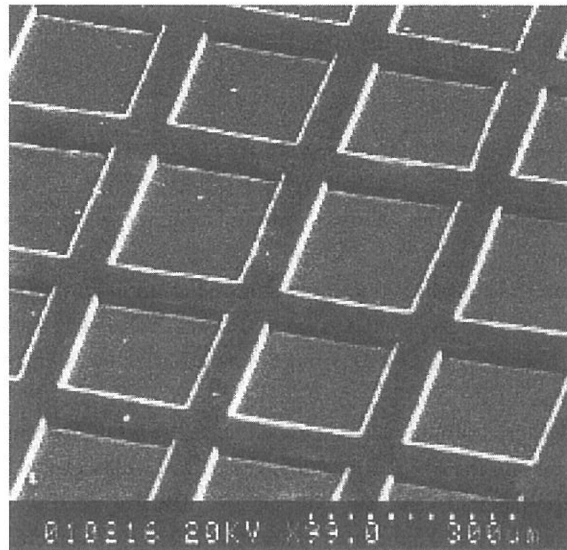

Figure 4. SEM image of PMMA microstructures.

REFRENCES

[1] E. W. Becker, *et. al.*, *Microelectron. Eng.*, **4**, pp.35-42 (1986).
[2] H. Mekaru, *et. al.*, *UVSOR Activity Report*, 38 (1999).
[3] H. Mekaru, *et. al.*, *Rev. Sci. Instrum.*, **70**, 2601-2605 (1999).
[4] B. L. Henke, E. M. Gullikson, and J. C. Davis, Atomic Data and Nuclear Data Tables, **54**, 216 (1993).

(BL5B)

Measurements of Total Photo-Desorption Yields from Solid Krypton by Exciton Creation

Takashi Adachi, Satoshi Ishii, Takato Hirayama, Ichiro Arakawa and Makoto Sakurai*
Department of Physics, Gakushuin University , Mejiro, Toshima, Tokyo 171-8588.
**Department of Physics, Kobe University, Rokkodai-cho, Nada-ku, Kobe 657-8501.*

1. Introduction

Desorption induced by electronic transitions (DIET) of various kinds of particles from rare gas solids has been extensively studied in these 10 years [1]. Investigation of the desorption characteristics such as desorption yields, kinetic energies and angular distributions, will reveal the dynamics of the electronic excitations and the relaxations.

We reported the absolute photo-desorption yields from the surface of solid neon [2] and argon [3, 4] at excitonic excitation energy and revealed the main desorption channel by the quantitative analysis. For a thick neon film, the desorption yield was 1-2 atoms/photon by bulk exciton excitation and 2-10 atoms/photon by bulk ionization. These values were quantitatively explained by the internal sputtering mechanism. In the case of argon, the absolute photo-desorption yield was 0.05-0.1 atoms/photon by bulk exciton excitation. The results agreed with the calculated value using the classical molecular dynamics by Cui et al [5]. The dissociation of excimer in the bulk was found to play an important role in the desorption mechanism of argon.

Here, we present the preliminary results of the total photo-desorption yields from the surface of solid krypton. The "total" means that we detected all the krypton particles desorbed, i.e., atoms and clusters in ground, electronically excited, and ionized states. In this report, we show only the relative desorption yields because the absolute number of incident photon have not been measured in the wavelength range of the exciton creation energy for solid krypton (100-130 nm).

2. Experiments

The experimental procedure and set-up have been described in detail elsewhere [2] and are briefly summarized here. Experiments have been carried out at the beam line BL5B in UVSOR of the Institute for Molecular Science, Okazaki. A liquid helium cryostat was installed in an ultrahigh-vacuum chamber with a base pressure of 5×10^{-9} Pa. Krypton gas was introduced into the main vacuum chamber and was condensed on the surface of a platinum substrate attached to the liquid helium cryostat. The temperature of the sample was 6 K or lower. The thickness of a krypton film was calculated from the exposure on the assumption that the condensation coefficient of the krypton on the sample surface was unity. The film thickness was between 10 and 2400 atomic layers.

Desorption rate was calculated from the total pumping speed for krypton and the rise of the krypton partial pressure in the vacuum chamber during the irradiation of the sample. The pumping speed for krypton of a turbo molecular pump and the cold surface of the cryostat was 0.068 ± 0.01 m^3/s in total. The partial pressure of krypton was measured by a quadrupole mass spectrometer which was calibrated with an ionization gauge at each run of the experiment.

3. Results

Figure 1 shows the wavelength dependence of the total desorption yields for solid krypton. In case the film thickness is 10 atomic layers, a peak is observed at 125 nm which corresponds to the excitation energy of the first order surface exciton (S1(3/2)). For the film of 2400 atomic layers in thickness, additional peaks appear at the wavelengths corresponding to the first order bulk (B1, 122 nm (3/2), 114 nm (1/2)) excitons. The small shoulders at 110, 116 and 112 nm in the spectrum for 2400 atomic layers film are due to the creation of the second order bulk (B2(3/2)), the first order surface (S1(1/2)) and the second order surface (S2(3/2)) excitons, respectively. The background signal is mainly due to the ionization by the second order light from the monochromater.

The thickness dependencies of the desorption yields at each exciton excitation energy are shown in figure 2. The desorption yield at the surface exciton creation energy should have no thickness dependence because the "thickness of the surface" is constant for any thickness of the film, which was indeed the case for neon [2] and argon [3,4]. However, in figure 2, the desorption yield at the first order surface exciton (3/2) excitation energy gradually decreases with the increase of the thickness of krypton film. This decrease can be the contribution of the residual gas adsorption on the sample surface. To make a thick krypton film, the substrate was exposed to gaseous krypton with rather high pressure (~ 1×10^{-4} Pa) for more than 10 minutes. After the exposure, we had to wait for about 1 hour or more in order to get a low pressure (< 2×10^{-8} Pa), which was essential for a good signal to background ratio in the present experiments. The sample surface can be partly covered with the residual gas (H_2, H_2O, CO, etc.) during this period, which resulted in the decrease of the desorption yield. This very slow pressure decrease was not observed in the measurements for neon and argon, which is explained by the difference of their vapor pressure at the temperature of the cryostat which has a temperature distribution from 4.2 K to the room temperature.

The desorption yields at the bulk exciton creation energies increase with the thickness of krypton film and saturated at about 200 atomic layers. The saturated value for B1 (3/2) and B1 (1/2) is roughly estimated at 0.01~0.1 krypton/photon. The measurements of the absolute intensity of the incident light at the wavelengths of the exciton creation for krypton (100-130 nm) will be done in the next machine time, which will give the absolute desorption yield. This will make it possible to discuss the desorption mechanism quantitatively.

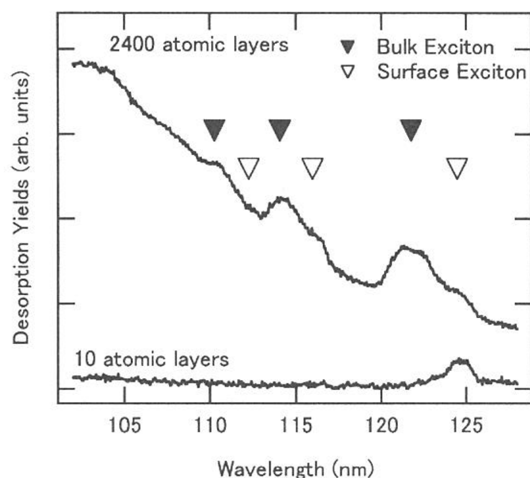

Fig.1 Wavelength dependence of total desorption yields of argon for thin (10 layers) and thick (2400 layers) films.

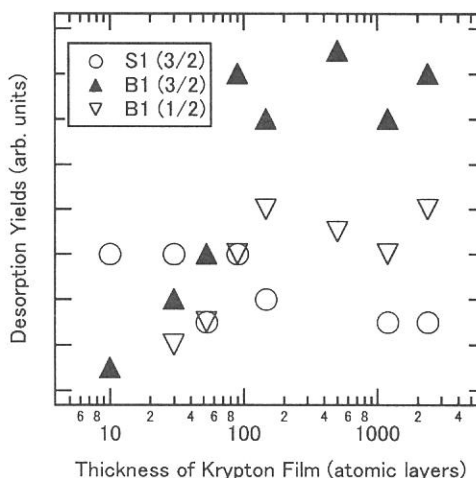

Fig.2 Thickness dependence of desorption yields at the bulk and surface exciton creation energies.

[1] for recent review, see I. Arakawa, Molec. Crystal Liq. Crystal, **314**, 47 (1998), M. Runne and G. Zimmerer, Nucl. Instrum. Meth. Phys. Res. B **101**, 156 (1995).
[2] I. Arakawa, T. Adachi, T. Hirayama and M. Sakurai, Surf. Sci. **451**, 136 (2000).
[3] T. Adachi, T. Hirayama, I. Arakawa and M. Sakurai, UVSOR Activity Report 1999, UVSOR-27, (2000) 178.
[4] T. Adachi, T. Hirayama, I. Arakawa and M. Sakurai, in preparation.
[5] S. Cui, R. E. Johnson, and P. Cummings, Surf. Sci. **207**, 186 (1988).

(BL-6B)

In-situ observation of synchrotron-radiation-stimulated process of surface reaction

Takafumi Tanaka[1,2] , Hideaki Yanagida[1,2], Kou Kurosawa[1] , Yoichi Nonogaki[1], and Tsuneo Urisu[1]

[1]Institute for Molecular Science, Okazaki, 444-8585 Japan

[2]Department of Electrical and Electronic Engineering, Miyazaki University, Miyazaki, 889-2192 Japan

Nano structures must open new windows not only for surface physics and chemistry but also for electronic and photonic devices. Synchrotron-radiation-stimulated surface chemical reactions have been a most promising way to fabricate nano structures, because they offer a process with the advantage of high-site selectivity by core electron excitation and also free-of damage with atomic scale. However, the detailed reactions have not been elucidated yet.

We have set and operated ultra-high vacuum scanning tunneling microscope (UHV-STM) and low energy electron diffraction (LEED) for atomic-resolution characterization of surfaces in the new beam line BL-6B. Figure 1 shows the outline of the beam line and observation system. The observation chamber is evacuated down to 1×10^{-10} Torr with turbo molecular, ion sputter, Ti-sublimation and NEG pumps. We have observed HOPG(0001) and Si(111) surfaces. We can obtain a clean surface of HOPG easily, but a clean surface of Si can not appear without sample heating, because the surface is covered with native oxide and carbonized layers. We have prepared the sample with wet chemical treatment called Shiraki method. By heating the sample to remove the layers, the clean surface is obtained. Figures 2 and 3 show the STM images of HOPG and Si surfaces. HOPG has been observed under such conditions that are scan width $1.5\times1.5\text{nm}^2$, scan speed 202nm/s,tunnel current 0.89nA, and bias voltage 0.089V. The conditions of Si are scan width $100\times100\text{nm}^2$, scan speed 3280nm/s, tunnel current 0.1nA, and bias voltage 2.0V. In the

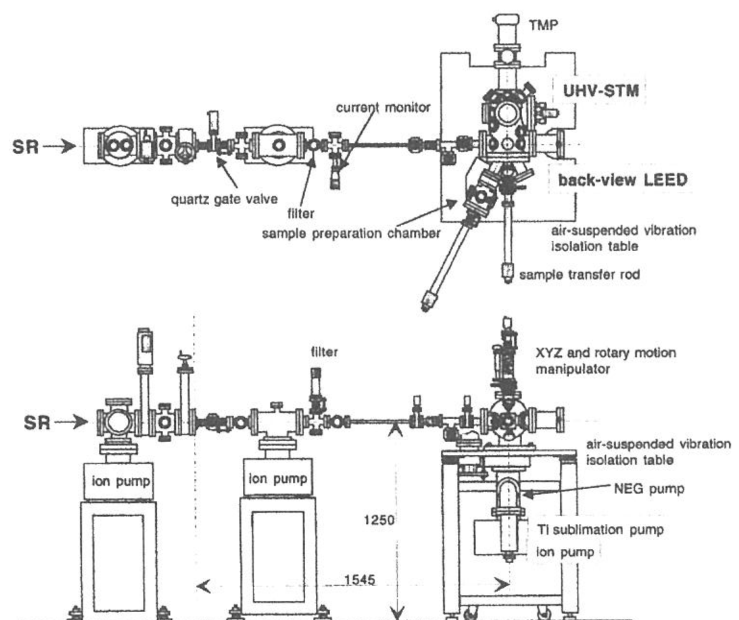

Figure 1. Schematic drawing of the BL-6B beam line and observation system.

figures, white appearing areas part correspond to the upper parts and black appearing ones are to the lower parts. In the case of the HOPG images, the atomic distances are found to agree with the theoretical values. In the case of Si images, steps with monoatomic height are shown in Figure 3. The LEED pattern inserted in the figure indicates that the Si(111) surface has a 7×7 reconstruction structure. At the present stage, the atomic images of Si(111) have not been obtained with STM yet. There is a problem in the system that the vacuum is not enough to keep Si (111) surfaces clean for a long time. Evacuating the preparation and observation chambers down to the order of 10^{-11} Torr and further optimize the observation conditions, we could observe the atomic images in the storage ring room on UVSOR.

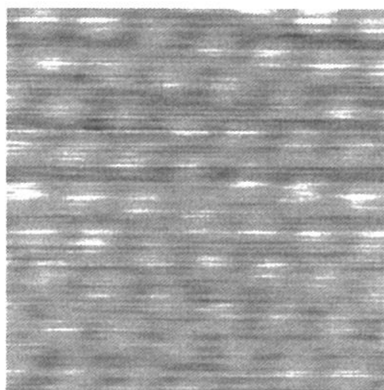

Figure 2. STM image of HOPG

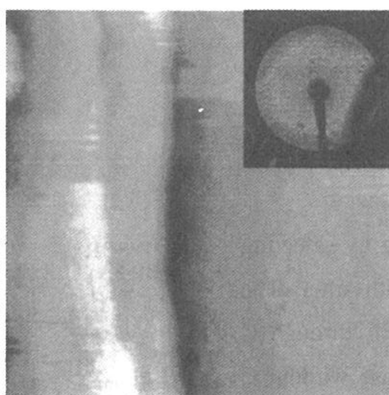

Figure 3. STM image of Si(111). The second insert of the LEED pattern.

(BL8A)

Investigation of Fragment from Polytetrafluoroethylene by Synchrotron Radiation Ablation

Hisao Nagai, Masaru Hori and Toshio Goto,
*Koji Katou and *Mineo Hiramatsu

Department of Quantum Engineering, Nagoya University, Chikusa-ku, Nagoya, 464-8603
**Department of Electrical and Electronic Engineering, Meijo University, Tempaku-ku, Nagoya, 468-8502*

INTRODUCTION

Fluorocarbon polymer has excellent properties such as chemical stability, potential biocompatibility and nonwetting property, and so on. Previously, we demonstrated the anisotropic micromachining and film formation of Teflon (fluorocarbon polymer) using synchrotron radiation (SR) ablation process [1,2]. Moreover, in order to clarify the mechanism of SR ablation, we have performed polytetrafluoroethylene (PTFE) micromachining by selecting the photon energy of SR beam with filter. From these results, we clarified that photon energies absorbed by carbon (C) and fluorine (F) atoms contribute to the ablation of PTFE. In this report, we have investigated the variation of fragments generated by PTFE ablation by quadraple mass spectroscopy (QMS).

EXPERIMENT

The experiments were carried out at beam line BL-8A of UVSOR. Figure 1 shows a schematic diagram apparatus used in this study. The PTFE target was set perpendicularly to the SR beam in the reaction chamber (base pressure of 10^{-4} Pa). A Nickel (Ni) mesh (square pattern of 77 μm) was used as the contact mask. The SR beam irradiated the samples through the Ni contact mask in vacuum at a room temperature. This experimental apparatus was equipped with QMS. In order to selecting the photon energy of SR beam, carbon (C) filter and C&MgFx filter was used. The thickness of C and C&MgFx filter were 100 nm, 200 nm, respectively. These filter were formed by electron beam evaporation.

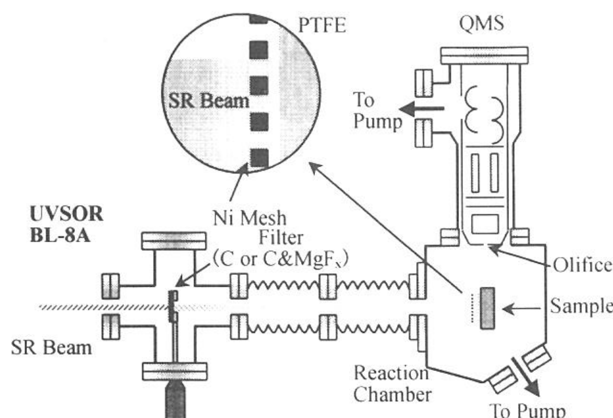

Fig. 1. Schematic diagram apparatus used in this study.

RESULTS AND DISCUSSION

We have performed PTFE etching by selecting the photon energy of SR beam with filter. The total photon flux irradiated on PTFE through C filter was the same as that in the case without C filter. As a result, the ablation rate with C filter was smaller than that of without C filter.

Figures 2 (a)-(b) show the QMS spectra of the fragments from PTFE target. Figure 2(a) shows

the QMS spectrum of CF fragment obtained from the target irradiated with white SR beam. Figure 2(b) shows the fragments after the SR beam passed through the C filter. These intensities were normalized to the maximum signal intensity (CF_3:Mass Number 69) and intensities of mass numbers above 70 was multiplied by 10 times. A big difference was not observed in the distribution of these spectra. Therefore, PTFE ablation with and without C filter would be identical in the ablation mechanism.

As shown Figs. 2 (a) and (b), the 69 fragment compared with the 31 fragment (CF) was dominated. T. Katoh *et al* reported that the domination at 69 indicated the main gaseous products by SR ablation should be the saturated fluorocarbon (CF_3-C_nF_{2n}-CF_3), while the domination at 31 indicated the main products are the monomers [3,4]. Thus, the domination at 31 would contribute to thermal decomposition of PTFE and domination at 69 would contribute to the saturated fluorocarbon generated by photochemical decomposition of PTFE irradiated SR beam. In this study, it is considered dominately reaction of SR ablation is photochemical decomposition.

SUMMARY

We have performed PTFE micromachining by selecting the photon energy of SR beam with filter and investigated the variation of fragments generated by PTFE ablation by QMS.

The dominate reaction of PTFE ablation by SR would be photochemical decomposition. The PTFE ablation with and without C filter would be identical in the ablation mechanism.

REFERENCES

[1] M. Inayoshi, M. Ito, M. Hori, T. Goto, M. Hiramatsu, and A. Hiraya, Jpn. J. Appl. Phys., **34**, L1675 (1995).

[2] M. Inayoshi, M. Ito, M. Hori, T. Goto, and M. Hiramatsu, J. Vac. Sci. Technol., **B 17**, 949 (1999).

[3] T. Katoh and Y. Zhang, Appl. Phys. Lett., **68**, 865 (1996)

[4] T. Katoh, Journal of Japan Society for Precision Engineering, **64**, 1008 (1998)

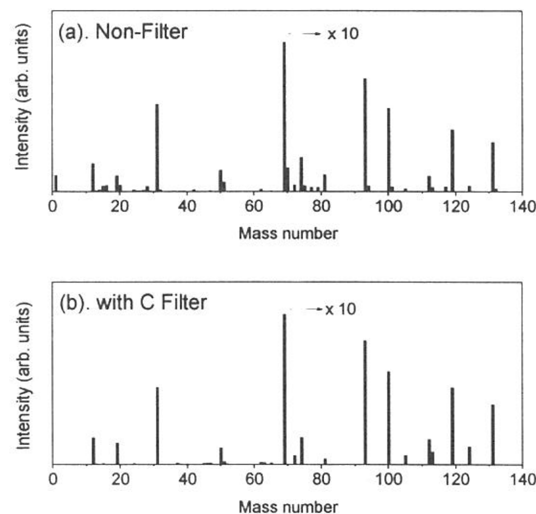

Fig. 2. QMS spectra of the fragments obtained from PTFE.
(a) fragment irradiated with white SR beam.
(b) passing SR beam through the C filter.

(BL8A)

Photoluminescence of ZnTe homoepitaxial films deposited by synchrotron-radiation-excited growth

Mitsuhiro Nishio, Kazuki Hayashida, Hiroki Harada, Toru Tanaka, Chiharu Ohata, Masahiko Tsujita, Yoshiaki Mitsuishi, Qixin Guo and Hiroshi Ogawa

Department of Electrical and Electronic Engineering, Saga University, Saga 840-8502, Japan

Synchrotron-radiation (SR) excited growth is promising as a new non-thermal technique, since virtually any reactants can be decomposed effectively at room temperature by using a high photon flux density in the vacuum ultraviolet region. Several attempts have so far been carried out using SR light to perform the deposition of semiconductors at low temperatures. In order to improve the film quality, it is important to investigate the photoluminescence (PL) spectrum of the film deposited by SR-excited growth. However, such investigations do not exist except for our previous papers, which described luminescence of ZnTe films grown using hydrogen carrier gas. In this study, we deal with PL properties of ZnTe films deposited by SR-excited growth technique using nitrogen carrier gas

The growth experiments were carried out using the SR beam line, BL8A. The beam line supplies only white light. Diethylzinc (DEZn) and diethyltelluride (DETe) were used as source materials. These source materials were independently fed into the chamber together with nitrogen carrier gas by means of mass flow controller and variable leak valve. The deposition of ZnTe was carried out at very low pressure of $10^{-5} \sim 10^{-4}$ Torr in the growth chamber. In order to clarify the effect of nitrogen carrier gas upon PL spectrum of the deposited film, the growth experiments have been carried out under almost the same growth conditions as the previous ones using hydrogen carrier gas.

We have found that there is no remarkable difference in the growth rate of the deposited film between hydrogen and nitrogen carrier gases. Thus, hydrogen seems not to play an important role in the growth reaction due to a use of the low pressure. However, we have discovered that PL spectrum of ZnTe film is significantly different from that in the case of hydrogen carrier gas. Figure 1(a) shows the PL spectra of ZnTe films for various source transport rates. In order to clarify the influence of carrier gas upon PL spectrum, the results in the case of hydrogen carrier gas are also shown in fig.1 (b). Here, we select samples corresponding to a Zn rich, nearly stoichiometric and Te rich conditions based on the growth rate behavior. It should be noticeable that in the PL spectrum of the film grown under a Zn rich condition, no deep level emissions can be detected whereas the PL spectrum of the film grown using hydrogen carrier gas exhibits strong deep level emissions with two broad bands centered at around 2.1 eV and 1.85 eV. The deep level emissions may be due to the generation of defects such as vacancy-impurity complex in the film. The deep-level luminescence obtained here can be found in the experimental results by Tews et al., who have attempted laser-induced diffusion in ZnTe with Cl.

As pointed out previously, in the case of hydrogen carrier gas, a Zn rich condition may facilitate Cl inclusion into a Te lattice site. Actually, a decrease of DEZn transports rate seems to bring about significant reduction of deep level bands. In the case of nitrogen carrier gas, a sharply excitonic emission (I_a) at 2.375 eV is detected prominently in the spectrum. This peak is attributed to shallow acceptors. Thus, a use of nitrogen carrier gas may be effective for suppression of deep level emission. It is well known that nitrogen is substituted on the Te lattice site and acts as a shallow acceptor. It is possible that nitrogen is included in the film and so participates shallow acceptors related to I_a peak. SR-excited growth may be effective for a use of thermally stable nitrogen as dopant, as shown in the growth of silicon nitride using nitrogen source. Similar feature can be found in the spectrum of the film grown under nearly stoichiometric condition. The appearance of strong I_a line may be due to a decrease in the numbers of deep-level centers such as Te vacancy complex accompanied by inclusion of nitrogen. On the other hand, the PL spectrum of the film grown under a Te rich condition exhibits new deep-level emission band in addition to I_a peak, as supported by the fact that the PL spectrum in the case of hydrogen carrier gas shows only donor-acceptor pair bands together with I_a line. Thus, a use of nitrogen carrier gas under a Te rich condition may bring about an increase in the numbers of deep-level centers such as Zn vacancy complex, different from the case of hydrogen carrier gas. Finally, we emphasize that near band gap luminescence can be observed even in the films grown at room temperature under Zn rich condition together with nearly stochiometric one by using nitrogen carrier gas.

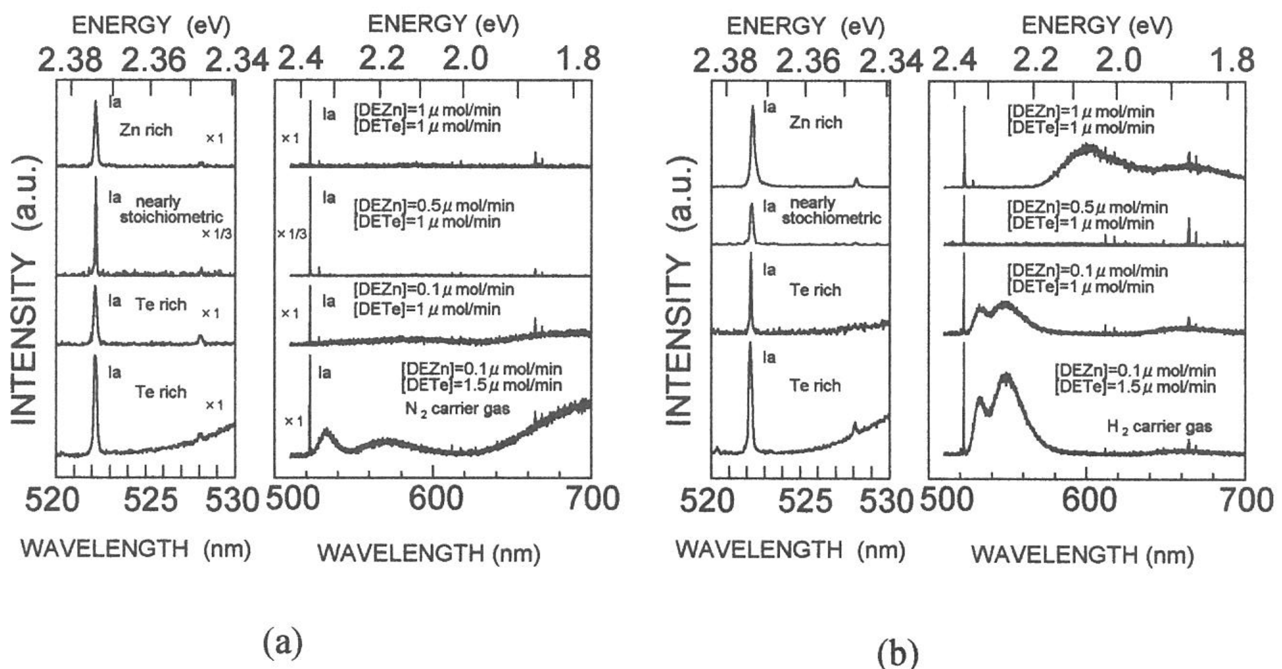

Fig. 1 PL spectra of ZnTe films for various source transport rates when substrate temperature was kept at 27℃. Fig. (a) corresponds to the case of nitrogen carrier gas, while fig. (b) the case of hydrogen carrier gas.

(BL8A)

Characterization of Polytetrafluoroethylene Thin Films Deposited by Synchrotron Radiation

M.Uchida, M.Ishizaka, H.Okada, A.Wakahara and A.Yoshida

Department of Electrical and Electronic Engineering, Toyohashi University of Technology, Tempaku, Toyohashi 441-8580

The polytetrafluoroethylene (PTFE) has been widely used in many application fields for a long time because of its unique properties such as chemical stability, thermal durability, hydrophobicity and low surface friction. Furthermore, electrical property of PTFE as the insulator is feasible for large-scale integrated circuits (LSIs) due to its low dielectric constant of ε_s=2.1 which value is smaller than that of SiO_2(ε_s=3.9). However, formation technique of the thin PTFE film having microscale pattern is not established yet. Recently, irradiation of the vacuum ultraviolet light from the SR beam is found to be useful for the micro processing of these materials in the small scale with very high rate even at room temperature.

In this report, we have investigated the deposition of PTFE by SR beam. Investigation was also made on the selective area etching of the PTFE with SR beam.

The experimental setup is shown in Fig.1. In the PTFE deposition experiment, PTFE target was put in the reaction chamber. A Si(100) substrate was placed in the position which countered with the target. The distance between target and the substrate is 3 cm. Before the deposition, the reaction chamber was evacuated below 1×10^{-6} Torr. With this setup, we investigated characteristics of the deposited films that were deposited with various beam current, target and substrate temperatures. Selective area etching of the deposited PTFE thin film was carried out by shadowing method. Here, we used the Ni mesh mask with the hole of $7.5\times7.5\,\mu$m and was closely placed on the PTFE thin film surface.

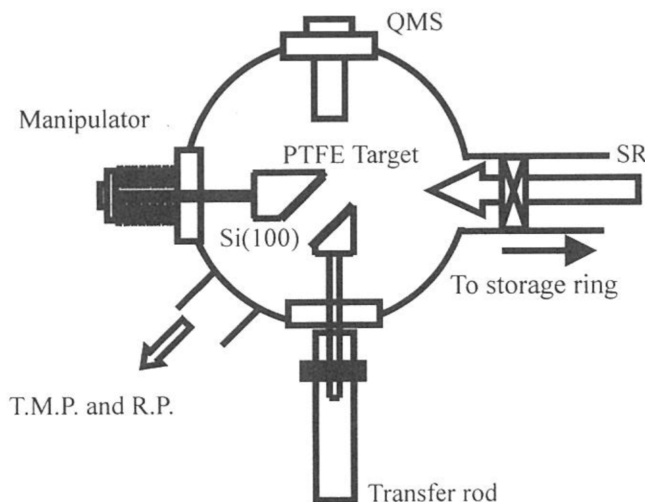

Fig.1 Experimental setup for deposition.

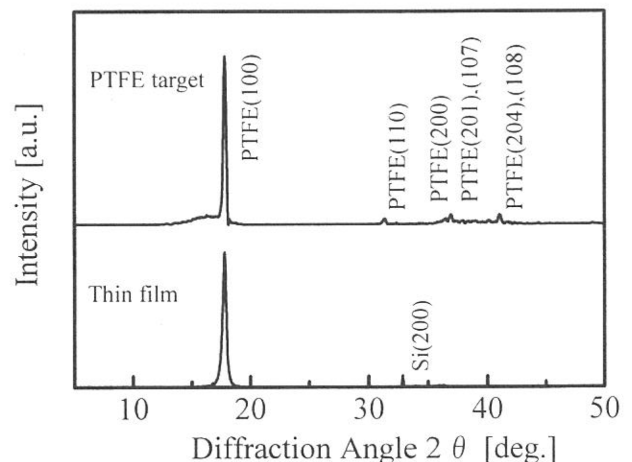

Fig.2 XRD spectra of PTFE target and PTFE thin film.

After the SR beam irradiation, we obtained PTFE deposition on Si substrate. Fig.2 shows XRD spectra of PTFE target and PTFE thin film deposited by SR beam. Both the PTFE target and the deposited thin film showed distinct peak at around 18° which was assigned to the peak from crystal portion of the PTFE. However, peak at 16° in the spectrum of the PTFE target was vanished in that of the deposited film. According to the previous report, sub-peak at around 16° indicates existence of the amorphous portion in the PTFE. Thus, better crystallinity of the PTFE thin film deposited by SR beam was demonstrated.

The surface morphology of the deposited PTFE thin film was characterized by atomic force microscope (AFM). AFM images of PTFE thin films deposited with beam current of 150 mA and 220 mA are shown in Figs.3(a) and 3(b), respectively, in range of 10 × 10 μm. In the case of the beam current of 150 mA shown in Fig.3(a), cracks are observed on the whole PTFE film surface. Depth of this cracks is in the range of 10 to 20 nm. On the other hand, as shown in Fig.3(b), such a crack is not observed on the PTFE film surface deposited with the beam current of 220 mA. These results indicate that smooth surface can be deposited with relatively large beam current. However, mechanism of the crack is not cleared yet. Further investigation is needed here.

Figure 4 shows a scanning electron microscope (SEM) image of selective area etched PTFE films by mesh shadowing method. Mesh patterned PTFE having sharp edge was obtained. Thus, selective area etching with SR beam exposure was succeeded.

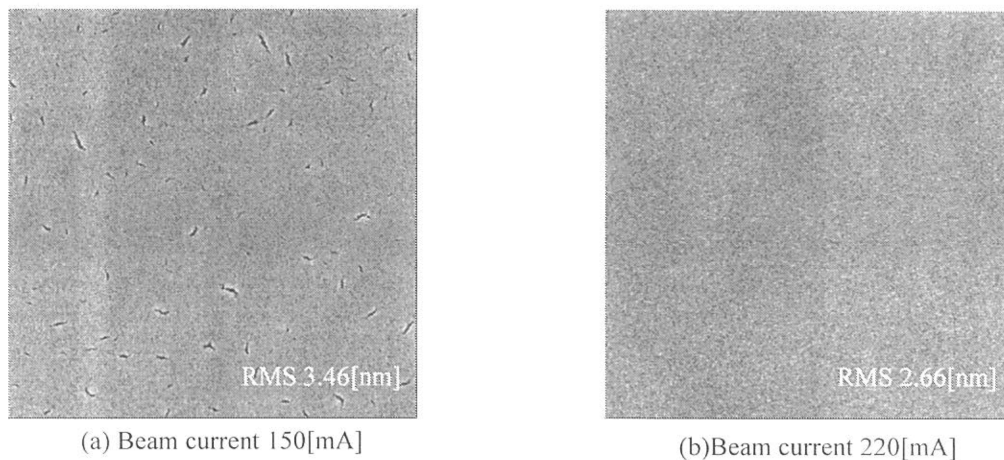

(a) Beam current 150[mA]

(b)Beam current 220[mA]

Fig.3 AFM images of PTFE thin film(10×10 μm).

(RMS was calculated in the portion without a crack.)

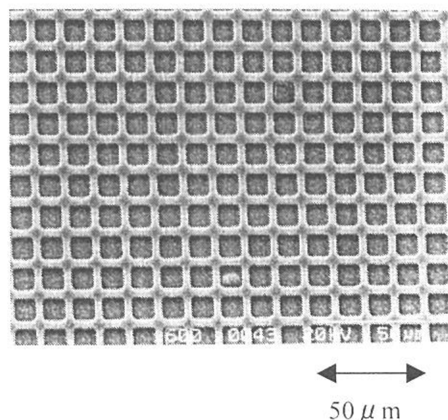

Fig.4 SEM image of selectively etched of PTFE thin film